

To appear in the Oct 2004 issue of *The Astronomical Journal*

**The Solar Neighborhood IX:
Hubble Space Telescope Detections of Companions to
Five M and L Dwarfs within 10 pc of the Sun**

David A. Golimowski,¹ Todd J. Henry,² John E. Krist,³ Sergio Dieterich,¹
Holland C. Ford,¹ Garth D. Illingworth,⁴ David R. Ardila,¹ Mark Clampin,⁵
Otto G. Franz,⁶ Lawrence H. Wasserman,⁶ G. Fritz Benedict,⁷ Barbara E. McArthur,⁷
and Edmund G. Nelan³

ABSTRACT

We report the detections of low-mass companions to five M and L dwarfs within 10 pc of the Sun using the *Hubble Space Telescope (HST)* Near-Infrared Camera and Multi-Object Spectrometer (NICMOS). Follow-up observations using the *HST* Advanced Camera for Surveys (ACS) and Fine Guidance Sensor 1r (FGS1r) confirm our NICMOS discoveries of companions to the L4.5 dwarf GJ 1001B (LHS 102B) and the M5 dwarf LHS 224, respectively. Images obtained with the Astrophysical Research Consortium 3.5 m telescope at Apache Point Observatory verify our discovery of a companion to the M3 dwarf G 239–25. Our NICMOS images confirm the previously suspected duplicity of the M3 dwarfs GJ 54 and GJ 84. The components of GJ 1001BC and LHS 224AB have nearly equal luminosities in all the ACS and/or NICMOS bandpasses in which they were observed. The magnitudes of GJ 54A and B in one FGS1r bandpass and four NICMOS bandpasses differ by $\lesssim 1$. GJ 84B and G 239–25B are ~ 4 magnitudes

¹ Department of Physics and Astronomy, Johns Hopkins University, 3400 North Charles Street, Baltimore, MD 21218-2686

² Department of Physics and Astronomy, Georgia State University, Atlanta, GA 30303-3083

³ Space Telescope Science Institute, 3700 San Martin Drive, Baltimore, MD 21218

⁴ Lick Observatory, University of California at Santa Cruz, 1156 High Street, Santa Cruz, CA 95064

⁵ NASA/Goddard Space Flight Center, Code 681, Greenbelt, MD 20771

⁶ Lowell Observatory, 1400 West Mars Hill Road, Flagstaff, AZ 86001

⁷ McDonald Observatory, University of Texas, Austin, TX 78712-1083

fainter than their M3 companions in the NICMOS bandpasses. We estimate from our NICMOS photometry that GJ 84B and G 239–25B have spectral types M7 and M8, respectively, and masses near the lower limit for sustained hydrogen burning. The apparent separations of GJ 1001BC, GJ 54AB, and LHS 224AB suggest orbital periods less than 5 yr. These binary dwarfs are ideal candidates for continued astrometric monitoring that will quickly yield accurate dynamic masses needed to constrain the mass–luminosity relation for low-mass stars and brown dwarfs.

Subject headings: binaries: close — stars: individual (G 239–25AB, GJ 1001ABC, GJ 54AB, GJ 84AB, LHS 224AB) — stars: low-mass, brown dwarfs

1. Introduction

Despite their proximity, the stars within 10 pc of the Sun remain an incompletely characterized population. This assessment is especially true for very-low-mass (VLM; $M \lesssim 0.20 M_{\odot}$) dwarfs, whose low luminosities ($L \lesssim 10^{-2.5} L_{\odot}$) retard comprehensive studies of their intrinsic properties and numerical abundance. For example, the empirical mass–luminosity relation (MLR) for late-M dwarfs is only sparsely sampled (Henry & McCarthy 1990, 1993; Henry et al. 1999; Delfosse et al. 2000), and its extension to the cooler L and T dwarfs is completely uncharted. Also, the luminosity function (LF) of the nearest VLM stars is unsettled, as M dwarfs within 10 pc continue to be identified as companions (Golimowski et al. 1995; Gizis & Reid 1996; Delfosse et al. 1999; Oppenheimer et al. 2001; this paper) and in isolation (Henry et al. 1997; Scholz, Meusinger, & Jahreiss 2001; McCaughrean, Scholz, & Lodieu 2002; Reid et al. 2003; Teegarden et al. 2003; Hambly et al. 2004). Only by exhaustively searching for faint nearby stars and closely-separated companions can the MLR and LF be sufficiently well determined to yield a definitive mass function of VLM stars and brown dwarfs.

Since July 1997, we have conducted a “snapshot” search for VLM companions to all known stars within 10 pc using the *Hubble Space Telescope* (*HST*) Near-Infrared Camera and Multi-Object Spectrometer (NICMOS). Our search spans the circumstellar region $0''.2$ – $10''$ from each target star, which corresponds to 2–100 AU for the most distant stars in our sample. This region bridges the 0–10 AU search-spaces of speckle-interferometry and radial-velocity surveys (Henry & McCarthy 1990; Leinert et al. 1997; Marcy & Butler 1998; Marcy, Cochran, & Mayor 2000) and the 100–1000 AU search-spaces of deep, near-infrared imaging surveys (Skrutskie, Forrest, & Shure 1989; Simons, Henry, & Kirkpatrick 1996; Kirkpatrick et al. 2001; Wilson et al. 2001; Hinz et al. 2002; McCarthy & Zuckerman 2004). With ultimate

detection limits of $M_J \approx 21$ and $M_K \approx 19.5$ at 10 pc (Krist et al. 1998), our NICMOS search is sensitive to companions that are at least 10 magnitudes fainter than the empirical end of the hydrogen-burning main sequence (Henry & McCarthy 1993) and at least 6 magnitudes fainter than the archetypal T dwarf, GJ 229B (Matthews et al. 1996; Leggett et al. 2002a).

The targets in our NICMOS snapshot program have been observed sporadically over seven years in order to fill small (~ 20 min) gaps in the *HST* observing schedule. To date, single-epoch images of 239 stars in 191 systems have been recorded. These observations represent 72% of the *HST* pointings required to survey all the stars and brown dwarfs within 10 pc identified astrometrically before 1 January 2004. (We treat known systems with separations less than $4''$ as individual *HST* targets.) In this paper – the ninth of the “The Solar Neighborhood” series produced by the Research Consortium on Nearby Stars (RECONS)¹ – we report the discoveries of VLM companions to three nearby M and L dwarfs (G 239–25, GJ 1001B, and LHS 224) and we confirm companions to two other M dwarfs (GJ 54 and GJ 84). All but one of these binary dwarfs have projected separations less than 5 AU. We discuss the potential impact of these companions on the MLR, and we update the state of multiplicity among presently known members of the RECONS “10 pc sample.”

2. Observations and Data Processing

Table 1 contains basic information about the five M and L dwarfs to which we report newly discovered or confirmed VLM companions. Information about GJ 1001A (also known as LHS 102A) is also included to provide a full description of the GJ 1001 system. Table 2 is a log of initial and follow-up observations of each dwarf conducted with NICMOS, the *HST* Advanced Camera for Surveys (ACS) and Fine Guidance Sensor 1r (FGS1r), and the Astrophysical Research Consortium (ARC) 3.5 m telescope at Apache Point Observatory. We now describe these observations in detail.

2.1. NICMOS Observations

Each dwarf was observed at a single epoch with NICMOS Camera 2 (NIC2), which has a pixel scale of $0''.076$ and a field-of-view (FOV) of $19''.5 \times 19''.5$ (Royer et al. 2003). The dwarfs were acquired as close to the center of the NIC2 field as the uncertainties in their coordi-

¹Information about RECONS is currently available on the World Wide Web at <http://www.chara.gsu.edu/RECONS/>.

nates and proper motions allowed. Images were recorded in fine-guidance mode through the F110W, F180M, F207M, and F222M filters (Table 3), which alternately sample the 1–2.5 μm spectra of putative brown-dwarf companions outside and inside the CH_4 absorption bands at 1.6–1.8 μm and 2.2–2.4 μm . Figures 1a and 1b show that this combination of filters permits easy discrimination of late-M, L, and T dwarfs from most background stars. We use this color discrimination and expectations based on Galactic latitude to identify candidate VLM companions among the many faint sources often imaged in a target field.

Images through each filter were recorded using NICMOS’s multiple-accumulate (MULTIACCUM) mode, which allows the detector to be read nondestructively in predefined sampling sequences. Two sets of exposures totalling 64 s were recorded through each of the F110W and F180M filters, and two sets of exposures totalling 128 s were recorded through each of the F207M and F222M filters. All sets of exposures were recorded using a logarithmic sampling sequence that provides large dynamic range among the constituent images. The images were reduced using the standard NICMOS calibration software (Dickinson et al. 2002) and appropriate reference images and tables. The calibration software combines the constituent images of each sampling sequence so that values of pixels ultimately affected by cosmic-ray impacts or saturation are replaced by appropriately scaled values of those pixels sampled before the contaminating event. Consequently, the lost data in the reduced images are limited to intrinsically bad pixels and/or pixels that were saturated before the first nondestructive read of the detector (i.e., within the first 0.303 s of the exposure). Figure 2 shows the set of reduced and calibrated images obtained for a typical target, namely, the binary M dwarf GJ 84AB.

To facilitate the detection of faint companions in the reduced images, we subtracted the point-spread functions (PSFs) of the target stars in the manner described by Krist et al. (1998). First, we selected reference PSFs for each target and filter from the large collection of single-star images recorded during our snapshot survey. The reference PSFs for a given target were those that best matched not only the brightness, spectral type, and field position of the target, but also the location of NIC2’s migratory cold mask at the time of the observation. The reference PSFs were then iteratively shifted, scaled, and subtracted from the target images until the residuals were visually minimized. Figure 3 shows the results of this technique for the images of GJ 84AB shown in Figure 2. Our imaging and processing strategies yield sensitivities to faint companions that are dependent on the brightness of the target, the quality of the PSF subtraction, and the field position. Krist et al. (1998) reported our detection limits at various angular distances from representative targets whose PSF-subtracted images are of average quality.

We measured the apparent magnitudes of unsaturated and well-separated targets and

field sources using conventional aperture photometry. To convert instrumental count rates to Vega-based magnitudes, we used aperture corrections computed for our selection of NICMOS filters (Krist et al. 1998) and the conversion recipe described in the *HST* Data Handbook for NICMOS (Dickinson et al. 2002):

$$m = -2.5 \log(PHOTFNU \times CR \times [F_\nu(\text{Vega})]^{-1}) + ZP(\text{Vega}), \quad (1)$$

where *PHOTFNU* is the bandpass-averaged flux density for a source producing a count rate of 1 DN s⁻¹, *CR* is the count rate (in DN s⁻¹) of the observed source measured for an infinite aperture, *F_ν*(Vega) is the flux of a zero magnitude star with a Vega-like spectrum, and *ZP*(Vega) = 0.02 is the magnitude of Vega in all NICMOS bandpasses (Campins, Rieke, & Lebofsky 1985). Table 3 lists the values of *PHOTFNU* and *F_ν*(Vega) adopted for images obtained before and after the installation of the NICMOS Cooling System (NCS) in March 2002.

We computed the magnitudes of closely-separated point sources from model NIC2 PSFs that were generated using the Tiny Tim software package (Krist & Hook 2003) and then fitted to each overlapping image.² To verify the fidelity of this method, we compared the four-band magnitudes of 35–80 single stars obtained from fitted Tiny Tim PSFs with those of the same stars obtained via conventional aperture photometry. The fitted F207M and F222M magnitudes were, on average, indistinguishable from those obtained via aperture measurements. The fitted F110W and F180M magnitudes, however, differed from the aperture magnitudes by an average of +0.013 and –0.022 mag, respectively. We therefore corrected the F110W and F180M magnitudes of closely-separated sources by subtracting these average offsets. The root-mean-square (RMS) deviations between the model and aperture magnitudes of our single-star sample were ~ 0.08 mag for F110W and only ~ 0.03 mag for the other filters. This consistency encouraged us to estimate the magnitudes of overexposed targets using model PSFs fitted to the unsaturated parts of their images. We investigated this procedure using artificially saturated images of a well-exposed star. We found that the fitted PSFs yielded progressively fainter magnitudes as the numbers of saturated pixels increased. Consequently, we adjusted the model magnitudes of actual saturated images to compensate for the deficiencies noted from our simulations. These adjustments ranged from 0.01 mag for images with one saturated pixel to 0.10 mag for images saturated within one

²We used model PSFs instead of natural reference PSFs because Tiny Tim produces oversampled images that can be more accurately fitted to the overlapping and undersampled NIC2 images. The model PSFs were generated with five times the pixel resolution of NIC2, aligned and scaled to each imaged source and then binned to the nominal NIC2 resolution to assess the quality of the fit.

Airy radius. The uncertainties of the magnitudes of overexposed stars estimated in this manner are ~ 0.02 – 0.25 mag.

The locations of sources in the reduced images were determined from either the centroids of the photometric apertures or the pixel coordinates of the fitted model PSFs. We estimate that the uncertainties of the former method are 0.1 pixel per axis, and those of the latter method are 0.2 pixel per axis for the undersampled F110W images and 0.1 pixel per axis for the other filter images. (We double these uncertainties for images affected by saturation or bad pixels.) To determine the angular separations and position angles of the binary dwarfs, we adopted the x -axis and y -axis pixel scales for NIC2 derived by the Space Telescope Science Institute around the times of our observations.³ We estimate that the nominal $1''$ uncertainty in the coordinates of *HST* guide stars contributes a negligible error of $\sim 0''.6$ to our computed position angles.

Figure 4 shows representative NIC2 images of the five dwarfs to which we have detected new or suspected companions. The insets show magnified contour plots of the four systems separated by less than $0''.5$. GJ 1001BC, GJ 54AB, and LHS 224AB are only marginally resolved. The images of LHS 224AB in all four bands are affected by bad NIC2 pixels, and the F110W images of GJ 54AB and GJ 84A are saturated. The faint object located $1''.74$ to the southeast of GJ 1001BC is an extended source, presumably a background galaxy. Table 4 lists the NICMOS magnitudes and relative positions of the components of the five systems, which we determined in the manners previously described. The magnitudes and colors of these dwarfs are depicted as filled circles in Figures 1a and 1b so that they may be readily compared with the NICMOS photometry of other main-sequence stars and brown dwarfs.

2.2. Follow-up Observations

Our NICMOS snapshot program is designed to be a single-epoch, multiband survey of all stars within 10 pc. Determining whether these stars and any candidate companions have common proper motion (CPM) technically exceeds the scope of our program. Nevertheless, second-epoch observations of candidate companions may be planned at the expense of unobserved targets. Only 50% of snapshot observations are likely to be executed during an *HST* observing cycle, however, so these second-epoch observations are not guaranteed. Consequently, we sought more reliable means of confirming our candidates. We have confirmed four of the five candidate companions identified in this paper using two telescopes and three

³The pixel scales for each NICMOS camera are presently available on the World Wide Web at <http://www.stsci.edu/hst/nicmos/performance/platescale>.

instruments, none of which are NICMOS. We now describe these confirmatory observations in chronological order.

2.2.1. GJ 54AB and LHS 224AB

The apparent separations and brightnesses of GJ 54AB and LHS 224AB (Table 4) make them ideal targets for astrometric monitoring with *HST*'s FGS, which features white-light shearing interferometers capable of measuring the positions of close-binary systems with $\sim 0''.001$ precision (Nelán et al. 2003). GJ 54AB was observed with FGS1r in transfer (TRANS) mode on 2000 September 24 and 2003 June 13. The TRANS scans were recorded through the wide-band F583W filter. LHS 224AB was observed with the same instrument configuration on 2000 January 7 and 2003 October 30. The first FGS observation of LHS 224AB, which predates our NICMOS observation by three years, was conducted as part of an independent FGS search for multiplicity among nearby M dwarfs and white dwarfs (*HST* Program 8532). Both binary systems continue to be monitored with FGS as parts of *HST* Programs 9408, 9972, and 10104. The complete results of these monitoring programs will be presented in subsequent papers. In the meantime, we present two-epoch results that support the duplicity of GJ 54 and LHS 224 inferred from our NIC2 images.

The TRANS-mode observations of each binary star were calibrated and processed in the manner described by Franz et al. (1991). Figure 5 shows the transfer functions of GJ 54AB, LHS 224AB, and the single star HIP 28355, measured along orthogonal axes of FGS1r. These X and Y transfer functions track the visibility of the broadband fringes as the stars are scanned across the Koester's prism (Franz et al. 1992). The transfer functions of a single star (left panels of Figure 5) are generally antisymmetric about the zero scan position that denotes alignment between the incoming wavefront and the optical axis. The transfer function of a binary star along a given FGS axis is the superposition of the individual stars' transfer functions, offset by their projected separation along that axis. The transfer functions of LHS 224AB recorded on 2003 October 30 (right panels of Figure 5) show that the binary star's orientation was nearly parallel to the Y -axis of FGS1r and its separation was $\sim 0''.16$. Likewise, the middle panels of Figure 5 show that, on 2003 June 13, GJ 54A and B were separated by $\sim 0''.13$ and were oriented obliquely to FGS1r's X and Y axes.

Decomposing the X and Y transfer functions of GJ 54AB and LHS 224AB into their constituent transfer functions allows us to determine the relative positions and F583W magnitudes of their components (Franz et al. 1991). Table 5 lists our preliminary results. The differences between the F583W magnitudes can be transformed to Johnson V -band magnitude differences (ΔV) in the manner described by Henry et al. (1999). Employing this

technique, we estimate $\Delta V = 1.03 \pm 0.08$ and 0.29 ± 0.02 for GJ 54AB and LHS 224AB, respectively. These values reflect the averages of the measurements obtained along each FGS axis at two epochs of observation. Their errors include those associated with the deconvolution of the transfer functions, the photometric transformations, and the published parallaxes and composite V magnitudes of each system.

2.2.2. *G 239–25AB*

Because the components of G 239–25 are relatively bright and widely separated (Table 4), follow-up observations of the system were possible using conventional ground-based imaging. We observed G 239–25AB on 2003 May 06 using the ARC 3.5 m telescope and the Seaver Prototype Imaging Camera (SPICam), which features a 2048×2048 -pixel CCD with an unbinned image scale of $0''.141 \text{ pix}^{-1}$. Exposures of 1 s, 10 s, and 60 s were recorded using the Sloan Digital Sky Survey (SDSS) z filter and 2×2 pixel binning. The 1 s image of G 239–25A was unsaturated and indicated a seeing-limited image resolution of $1''.25$. The sky transparency was variable, so no photometric calibration was possible. The images were reduced conventionally by subtracting the electronic bias and dividing by a flat-field image.

Figure 6 shows a $14''.4 \times 14''.4$ section of the the reduced 1 s image centered on G239–25A. Part of the star’s seeing-limited PSF has been subtracted to reveal G239–25B more clearly. [Lacking a comparably exposed reference star, we subtracted artificial background values that were interpolated from radial profiles of the PSF at azimuths $\pm 45^\circ$ from the position angle (PA) of G239–25B.] The companion is located $2''.84 \pm 0.14$ from G 239–25A at $\text{PA} = 106^\circ.5 \pm 3^\circ.6$. The errors in these values include a 0.5 pixel uncertainty in each coordinate of G 239–25B’s centroid and a possible $0^\circ.4$ error in the alignment of SPICam’s detector with the celestial axes (R. McMillan 2004, private communication). The integrated signals of each star within circular apertures of radius $0''.85$ (3 pixels) indicate a magnitude difference of $\Delta z \approx 4.9$.

2.2.3. *GJ 1001ABC*

A follow-up observation of the GJ 1001 triple system was performed on 2003 August 20 using the High Resolution Channel (HRC) of the *HST* ACS (Ford et al. 2003; Pavlovsky et

al. 2003).⁴ The HRC features a 1024×1024 -pixel CCD with a pixel scale of $\sim 0''.025 \times 0''.028$. Its $\sim 26'' \times 29''$ FOV allowed simultaneous imaging of all three components of the system. Two sets of 2 s, 60 s, and 300 s exposures were recorded through the F850LP (SDSS z) filter to allow unsaturated imaging of each component. Between exposures, the telescope was offset by ~ 6.5 pixels along each CCD axis to diminish the possibility of image corruption by bad pixels. Likewise, two sets of 2 s and 300 s exposures were recorded through the F625W (SDSS r) and F775W (SDSS i) filters. All exposures were recorded using an analog-to-digital conversion gain of $2.2 e^- \text{ DN}^{-1}$. The digitized images were bias-subtracted and flattened using the standard ACS calibration software (Mack et al. 2003) and appropriate reference images and tables. The flattened images were then processed with the ACS Pipeline Science Investigation Software (APSYS; Blakeslee et al. 2003) to remove cosmic-ray contaminants, correct the images for geometric distortion, and combine the dithered pairs of images. The reduced and resampled HRC images have rectified pixel scales of $0''.025$ along each axis.

Figure 7 shows the resultant 2×300 s F775W image of GJ 1001ABC. Although GJ 1001A is overexposed in this image, it is suitably exposed in our 2 s F775W images. These levels of exposure are also characteristic of the images obtained with the F625W and F850LP filters. The binary L dwarf is clearly resolved, and its photocenter lies $\sim 18''.2$ from GJ 1001A at $\text{PA} \approx 259^\circ$. These values are consistent with the relative positions of GJ 1001A and B reported by Goldman et al. (1999) from lower resolution, ground-based images in which GJ 1001A is overexposed.

Although the angular resolution of the HRC at $\lambda = 0.9 \mu\text{m}$ is ~ 2.2 times better than that of NIC2 at $\lambda = 1.1 \mu\text{m}$, the HRC images of GJ 1001B and C overlap sufficiently to preclude the use of aperture photometry. Consequently, we generated model PSFs for each component using Tiny Tim (Krist & Hook 2003) and a reference spectrum of the L4 dwarf 2MASS J03454316+2540233 (Geballe et al. 2002). Because Tiny Tim produces only geometrically distorted PSFs, we fitted model PSFs to the flattened but distorted (i.e., pre-APSYS) images of GJ 1001B and C. Tiny Tim does not fully simulate the diffuse halo of scattered light that is superposed on point-source images longward of $\sim 0.8 \mu\text{m}$ (Sirianni et al. 1998), so we derived approximate corrections for this effect in the F775W and F850LP bandpasses for each dwarf. In doing so, we normalized the integrated pixel values from the PSFs fitted to the images of GJ 1001A with those obtained directly from the APSIS-processed images using circular apertures with radii of $0''.5$ and the aperture corrections for M dwarfs reported by Sirianni et al. (2004). We then applied the same normalization to the PSFs fitted to the images of GJ 1001B and C along with additional corrections of

⁴This observation was conducted as part of the guaranteed observing time awarded to the ACS Investigation Definition Team.

$\Delta m_{F775W} = -0.008$ and $\Delta m_{F850LP} = -0.057$ to compensate for the spectral differences between GJ 1001A and GJ 1001BC (Sirianni et al. 2004). We also applied small ($\sim 1\%$) corrections for photometric losses caused by CCD charge-transfer inefficiency (Riess 2003). We estimate that the uncertainties of these corrected count rates are $\sim 4\text{--}8\%$. We converted the count rates to AB and Vega-based magnitudes using the photometric calibration recipe of Sirianni et al. (2004), which specifies that Vega has zero magnitude in all bandpasses. Table 6 lists the resulting magnitudes and errors of GJ 1001ABC in each bandpass.

To determine the relative separations and orientations of the system components, we transformed the pixel coordinates of the fitted PSFs (which are measured from the geometrically distorted images) to angular coordinates measured along the V2 and V3 axes that define *HST*'s principal focal plane. In doing so, we used the latest image-distortion correction table (IDCTAB) for the HRC, which has an RMS residual error of 0.03–0.05 pixels per axis for the filters used in our study (Meurer et al. 2002). The errors in the measured centroids of our fitted PSFs are ~ 0.1 pixel, and the uncertainty in the orientation of the HRC FOV due to the $\pm 1''$ inaccuracy of *HST* guide star coordinates is $\pm 0''.7$. Columns 6–8 of Table 6 list the apparent and projected separations and position angles of the GJ 1001 system, based on the average measurements from individual HRC images and the parallax given in Table 1. The first set of values pertains to the separation and orientation of the photocenter of GJ 1001BC with respect to GJ 1001A. The second set of values pertains to components B and C separately.

3. Discussion

The PSF-subtracted NIC2 images of each dwarf reveal no sources other than the five companions and the single galaxy in the field of GJ 1001BC. The paucity of background sources is not surprising given the generally high Galactic latitudes of the dwarfs (col. 4 of Table 1) and NIC2's small FOV. Thus, the dwarfs' high latitudes raise the likelihood that any apparent companions are true companions. Indeed, the high latitudes of these dwarfs prompted their inclusion in this paper announcing the first confirmed companions of our NICMOS survey. We now discuss the evidence confirming these companions and the implications for our future understanding of VLM multiple systems. We begin with GJ 1001BC, which is arguably the most significant of the newfound binaries from the perspective of constraining the MLR in the substellar regime.

3.1. GJ 1001ABC

Assuming that GJ 1001C is always the fainter of the close-binary components seen in our NIC2 and HRC images, then GJ 1001C moved $\sim 0''.07$ at PA $\sim 164^\circ$ relative to GJ 1001B during the 313 days between our epochs of observation. This motion is much less than that expected from the annual proper motion of the GJ 1001 system ($1''.618$ at PA = $154^\circ.5$; van Altena, Lee, & Hoffleit 1995). However, the NIC2 magnitudes of GJ 1001B and C differ by amounts similar to their combined uncertainties, so their identities at each epoch are somewhat ambiguous. If we switch their identities in the NIC2 images, then GJ 1001C moved $\sim 0''.16$ at PA $\sim 72^\circ$ relative to GJ 1001B between our NICMOS and ACS observations. This motion is also much smaller and differently oriented than the annual proper motion of the GJ 1001 system. Conversely, the photocenter of GJ 1001BC moved $1''.41$ at PA = $153^\circ.6$ relative to the galaxy labeled in Figure 7, which is consistent with the annual proper motion. We therefore conclude that GJ 1001A, B, and C have CPM regardless of how the components are labeled, and that the relative motion of GJ 1001B and C is orbital in nature.

Using the observed separations of GJ 1001BC, a distance to the triple system of $d = 9.55 \pm 1.04$ pc (van Altena, Lee, & Hoffleit 1995), and the statistical relation between the observed angular separation (α) and the semimajor axis of the relative orbit (a_{rel}),

$$\langle a_{\text{rel}} \rangle = 1.26 d \langle \alpha \rangle \quad (2)$$

(Fischer & Marcy 1992), we estimate that $a_{\text{rel}} \approx 1.04 \pm 0.12$ AU. The age of GJ 1001A is loosely constrained to 1–10 Gyr (Leggett et al. 2002b; Gizis, Reid, & Hawley 2002), so we infer from evolutionary models (Burrows et al. 1997; Chabrier et al. 2000) that its coeval L4.5 dwarf companions ($T_{\text{eff}} \approx 1750$ K; Golimowski et al. 2004) have masses of 0.06–0.075 M_\odot . If so, then the period of GJ 1001BC’s orbit is $\sim 2.9 \pm 0.5$ yr, which is the shortest estimated period of any known binary L or T dwarf (Table 7). However, the $\sim 47^\circ$ (clockwise) difference between the position angles of GJ 1001C in the NIC2 and HRC images suggests either that the orbital period is actually much longer than 3 yr, or that GJ 1001B and C are not consistently identified in the NIC2 and HRC images. If the identities of GJ 1001B and C in the NIC2 images are switched, then GJ 1001C’s position angle changed by $\sim 133^\circ$ (anticlockwise), which is more compatible with a ~ 3 yr period than the motion inferred from our adopted designations of GJ 1001B and C.

Since its discovery in 1999, GJ 1001B has been well studied photometrically and spectroscopically (Goldman et al. 1999; Basri et al. 2000; Leggett et al. 2002b). As a companion to an M dwarf of known distance, it has frequently been used to study the relationships

between the luminosities, colors, and spectral types of L dwarfs (Kirkpatrick et al. 2000; Dahn et al. 2002; Knapp et al. 2004; Golimowski et al. 2004). None of these studies describes GJ 1001B as overluminous for its color or spectral type, as would be expected for a non-eclipsed binary system with components of equal luminosity. The fact that GJ 1001BC is binary indicates that either its components are underluminous or its inferred trigonometric parallax is incorrect. The composite optical and near-infrared spectra of GJ 1001BC show that the components are typical mid-L dwarfs and reveal no cause for underluminosity in any optical or near-infrared bandpass. Applying the SDSS color–magnitude relation of Hawley et al. (2002) to our ACS photometry of each component (Table 6), we compute an average photometric parallax of $0''.046 \pm 0''.017$, or a distance to GJ 1001BC of 21.8 ± 7.9 pc. Similarly applying the spectroscopic parallax relations of Hawley et al. (2002) for L4.5 dwarfs, we obtain distance moduli of $M-m \approx -0.4$ to -0.7 , or $d \approx 12$ – 14 pc. Although these estimated photometric and spectroscopic distances agree only marginally, both suggest that the only published trigonometric parallax of GJ 1001A (van Altena, Lee, & Hoffleit 1995) is too large. Indeed, preliminary astrometric results for GJ 1001A from the Cerro Tololo Parallax Investigation indicate that the star’s distance is closer to 15 pc than to 10 pc (T. Henry et al., in preparation).

Assuming a revised distance of ~ 15 pc to GJ 1001BC, we estimate that its relative orbit has a semimajor axis of ~ 1.6 AU and a period of ~ 5.5 yr. Unfortunately, the uncertainties associated with these estimates prevent us from identifying GJ 1001B and C in the NIC2 images unambiguously. Regardless of the components’ designations, GJ 1001BC offers a superb opportunity to determine the orbit and dynamical masses of two probable brown dwarfs in a small amount of time. Our HRC images show that *HST* can provide the high-resolution images necessary for such pioneering measurements, if its lifetime is extended by a fifth servicing mission. GJ 1001BC’s faintness and small separation pose a challenge for ground-based telescopes equipped with adaptive optics (AO), but the image resolution achieved during recent AO observations of the binary T dwarfs ϵ Indi BC (McCaughrean et al. 2004) indicate that long-term monitoring of GJ 1001BC’s orbit should be possible with the latest ground-based imaging technology.

3.2. GJ 54AB

The suspected duplicity of GJ 54 was first reported by Rodgers & Eggen (1974), who visually observed a “very close double star of nearly equal components in the 40-inch reflector” at Siding Spring Observatory. They provided no information about the separation of the double star or the epoch of their observation, but the lack of other stars of comparable

brightness within several arcminutes of GJ 54 suggests that Rodgers & Eggen did observe the same pair of stars seen in our NIC2 images. The V -band diffraction limit of a 40-inch telescope is comparable to the separation of GJ 54AB measured from our NIC2 and FGS data, so Rodgers & Eggen may have seen the pair during instances of excellent atmospheric seeing. Therefore, we credit Rodgers & Eggen (1974) with the initial discovery of GJ 54AB, and reserve for ourselves the pleasure of confirming and quantifying that discovery.

The FGS TRANS scans of GJ 54 recorded on 2000 September 24 and 2003 June 13 (Figure 5) show two components separated by $\sim 0''.12$ (Table 5). This separation is similar to that measured from our NIC2 images obtained on 1998 November 9, and it is much less than GJ 54’s annual proper motion of $0''.692$ (ESA 1997). We therefore conclude that GJ 54A and B exhibit CPM and are physically bound. Figures 1a and 1b show that the NIC2 magnitudes and colors of GJ 54A and B are consistent with other stars in our 10 pc sample having spectral types M2.0–M2.5 and M3.0, respectively. Using our computed value of ΔV for GJ 54AB (§2.2.1) and published measurements of the stars’ composite V magnitude and parallax (Table 1), we obtain $M_V = 10.60 \pm 0.11$ and $M_V = 11.63 \pm 0.12$ for GJ 54A and B, respectively. Employing the V -band MLR of Delfosse et al. (2000), we compute masses of $0.42 \pm 0.07 M_\odot$ and $0.31 \pm 0.07 M_\odot$ for the two stars.

Using our *HST* measurements, a distance to GJ 54AB of 8.20 ± 0.41 pc (Table 1), and equation (2), we estimate a semimajor axis of 1.33 ± 0.09 AU and a period of 1.8 ± 0.2 yr for GJ 54AB’s relative orbit. After deconvolving the individual components of the FGS transfer functions and transforming them to celestial positions, we find that the position of GJ 54B relative to GJ 54A on 2000 September 24 was nearly coincident with the position observed in the NIC2 images recorded 1.87 yr before. In fact, a preliminary fit of a Keplerian orbit to our three-epoch astrometric measurements yields a highly inclined orbit with a semimajor axis of $\sim 0''.17$ (~ 1.4 AU), a period of ~ 1.75 yr, and masses of $0.49 M_\odot$ and $0.33 M_\odot$. Thus, our crude photometric and astrometric estimates of the orbits and masses of GJ 54AB are mutually consistent.

3.3. GJ 84AB

Nidever et al. (2002) reported 11 radial-velocity measurements of GJ 84 obtained at the 10 m Keck I Observatory from 1998 February to 2001 July that indicate the presence of a low-mass companion. They reproduced the velocity variations by fitting a partial Keplerian orbit with a period of 19 ± 7 yr, a semiamplitude of 2.2 ± 0.2 km s $^{-1}$, and an eccentricity of 0.44 ± 0.08 . They also estimated for the companion a minimum mass of $0.115 M_\odot$ and a minimum semimajor axis of 5.6 AU. These values are consistent with the luminosity and

projected separation of the faint companion seen in our NIC2 images (Table 4). Our images thus confirm the duplicity of GJ 84, and are useful for further constraining the parameters of the binary orbit.

Figure 1b shows that the values of $M_{\text{F110W}} = 11.10 \pm 0.10$ and $\text{F110W–F222M} = 1.58 \pm 0.10$ measured for GJ 84B lie between those of the M7 dwarf GJ 105C ($M_{\text{F110W}} = 10.93$, $\text{F110W–F222M} = 1.42$; revised from Golimowski et al. 2000) and the M8 dwarf GJ 752B ($M_{\text{F110W}} = 11.59$, $\text{F110W–F222M} = 1.71$). The anomalous location of GJ 84B’s colors in Figure 1a is likely due to a singularly large error in our F180M measurement caused by the coincidence of GJ 84B’s image and a diffraction spike from GJ 84A (Figures 2 and 3). As the magnitudes and colors of GJ 84B generally match those of GJ 105C within their combined uncertainties, we tentatively assign a spectral type of M7 to GJ 84B. To estimate the masses of GJ 84A and B from current near-infrared MLRs, we loosely equate our measured values of M_{F110W} and $\frac{1}{2}(M_{\text{F207M}} + M_{\text{F222M}})$ for each star with its conventional J - and K -band absolute magnitude, respectively. Employing the MLRs of Delfosse et al. (2000), we obtain masses of $0.51 \pm 0.06 M_{\odot}$ and $0.084 \pm 0.026 M_{\odot}$ for GJ 84A and B, respectively. Using these masses, a distance to GJ 84AB of 9.40 ± 0.17 pc (Table 1), the observed binary separation (Table 4), and equation (2), we estimate a semimajor axis of 5.25 ± 0.12 AU and a period of 15.6 ± 1.0 yr for GJ 84AB’s relative orbit.

We can investigate the consistency between the orbital characteristics estimated from our NIC2 images and those derived by Nidever et al. (2002) from the Keplerian fit to their measured radial velocities. Kepler’s Third Law may be expressed as

$$\frac{a_1}{\pi_{\text{abs}}} = P^{2/3} \frac{M_2}{(M_1 + M_2)^{2/3}} \quad (3)$$

(Lang 1980), where a_1 is the semimajor axis of the primary star’s orbit about the barycenter in units of arcsec, π_{abs} is the absolute parallax, P is the orbital period expressed in years, and M_1 and M_2 are the primary and secondary masses in units of M_{\odot} . Using our estimated masses of GJ 84A and B and the fitted radial-velocity period of Nidever et al. (2002), we obtain $a_1 \approx 0''.089 \pm 0''.035$. An equation relating orbital parameters derived astrometrically and spectroscopically (Lang 1980) can be expressed as

$$\frac{a_1 \sin i}{\pi_{\text{abs}}} = \frac{PK_1 \sqrt{1 - e^2}}{2\pi \times 4.7405}, \quad (4)$$

where i is the inclination of the orbit with respect to the line of sight, K_1 is the semiamplitude of the primary star’s radial-velocity orbit in units of km s^{-1} , e is the eccentricity of the orbit, and $\pi \approx 3.14159$. Inserting the values of a_1 , P , K_1 , and e derived by Nidever et al. (2002)

and us, we obtain $\sin i \approx 1.49 \pm 0.85$. Only the values of $\sin i$ deviating by more than -0.5σ from 1.49 are physical, which indicates that the Keplerian fit to the radial velocity data is only marginally compatible with our observed luminosities (masses) of GJ 84AB. Clearly, more spectroscopic and astrometric observations are needed over the next decade to better constrain the orbit of GJ 84AB.

3.4. LHS 224AB

The duplicity of LHS 224 was first suspected by Dahn et al. (1982), who noted a possible astrometric perturbation with a period of ~ 6 yr from photographic plates produced by the United States Naval Observatory from 1969 to 1980. After another decade of astrometric monitoring, Harrington et al. (1993) could neither confirm nor deny this suspicion. In 1999, LHS 224 was included in our ongoing FGS survey of nearby and possibly binary red and white dwarfs. The TRANS scans of LHS 224 recorded on 2000 January 7 and 2003 October 30 (Figure 5) show two components separated by $\sim 0''.16$ (Table 5). This separation is similar to that measured from our NIC2 images obtained on 2003 March 13, and it is much less than LHS 224’s annual proper motion of $1''.166$ (Gliese & Jahreiss 1991). We therefore conclude that LHS 224A and B exhibit CPM and are physically bound.

Figures 1a and 1b suggest that the NIC2 F110W magnitudes and F110W–F222M colors of LHS 224AB are brighter and bluer, respectively, than those of other M5 dwarfs. Such anomalous behavior is not seen in other color–magnitude and color–color diagrams constructed from our F180M, F207M, and F222M photometry of nearby stars. We therefore suspect that our F110W measurements are adversely affected by the undersampled F110W images of LHS 224AB and by the unfortunate proximity of bad pixels to those images (Figure 4). The magnitudes and colors of LHS 224A and B measured in the other bandpasses are consistent with those of several nearby dwarfs having types M4.5–M5.0 and M5.0–M5.5, respectively. Using our computed value of ΔV for LHS 224AB (§2.2.1) and published measurements of the stars’ composite V magnitude and parallax (Table 1), we obtain $M_V = 14.08 \pm 0.05$ and $M_V = 14.37 \pm 0.05$ for LHS 224A and B, respectively. Employing the V -band MLR of Delfosse et al. (2000), we compute masses of $0.16 \pm 0.02 M_\odot$ and $0.14 \pm 0.02 M_\odot$ for the two stars.

Using our NIC2 measurements, a distance to LHS 224AB of 9.2 ± 0.2 pc (van Altena, Lee, & Hoffleit 1995), and equation (2), we estimate $a_{\text{rel}} \approx 1.53 \pm 0.08$ AU and $P \approx 3.5 \pm 0.3$ yr for LHS 224AB’s orbit. A preliminary fit of a Keplerian orbit to our three-epoch astrometric measurements yields $a_{\text{rel}} \approx 1.6$ AU, $P \approx 3.3$ yr, and masses of $\sim 0.21 M_\odot$ and $\sim 0.20 M_\odot$. These dynamic masses exceed our photometric estimates by 3σ , but we

expect these discrepancies to diminish greatly as more FGS measurements are obtained over a broader range of orbital phases.

3.5. G 239–25AB

During the 4.5 years between our NIC2 and SPICam observations, G 239–25A’s proper motion was $1''.42$ toward $PA = 259^\circ.2$ (ESA 1997). The magnitude and direction of this motion are inconsistent with the small differences between the relative positions of G 239–25A and B at each epoch. We therefore conclude that G 239–25A and B have CPM and are gravitationally bound. Moreover, we believe that the observed motion of G 239–25B relative to G 239–25A ($0''.43 \pm 0''.14$ toward $PA = 352^\circ \pm 22^\circ$) is orbital in nature.

Figures 1a and 1b show that the NIC2 magnitudes and colors of G 239–25B are similar to those of the M8 dwarf GJ 752B and the spectroscopically unclassified late-M dwarf GJ 1245C. The latter dwarf is the least massive M dwarf ($0.074 \pm 0.013 M_\odot$; Henry et al. 1999) for which a mass has been computed exclusively from dynamical elements.⁵ We assume for our present purpose that G 239–25B has the same spectral type and mass as GJ 752B and GJ 1245C, respectively. Liberally applying our F110W, F207M, and F222M photometry of G 239–25A to the near-infrared MLRs of Delfosse et al. (2000; see §3.3 of this paper), we estimate a mass of $0.32 \pm 0.15 M_\odot$ for the M3 dwarf. Using these masses, a distance to G 239–25AB of 9.9 ± 1.2 pc (ESA 1997), the observed binary separations (Table 4 and §2.2.2), and equation (2), we estimate $a_{\text{rel}} \approx 37.8 \pm 4.8$ AU and $P \approx 370 \pm 100$ yr for G 239–25AB’s orbit.

If our estimates of the physical and dynamical characteristics of G 239–25AB are correct, then G 239–25A’s radial velocity should vary periodically with an amplitude of ~ 3 km s^{−1}. Nidever et al. (2002) reported that the radial velocity of G 239–25A (HIP 71898) was stable to within 0.1 km s^{−1} of 18.704 km s^{−1} over 864 days distributed about a mean calendar date of 1999 January 5. On the other hand, Upgren & Harlow (1996) reported that the star’s radial velocity increased from 17.51 to 21.17 km s^{−1} (with an average uncertainty of ± 1.22 km s^{−1}) over 68 days in mid-1994. This trend is hard to explain in the face of the more precise measurements of Nidever et al. (2002) and our estimated period of ~ 370 yr. The *Hipparcos* and Tycho Catalogues note that the large error associated with the G 239–25A’s parallax (Table 1) is consistent with the effects of a short-period astrometric binary (ESA 1997). However, subsequent reanalysis of the *Hipparcos* measurements yielded a “more

⁵Lane et al. (2001) mapped the relative orbit of the M8.5+M9 dwarf binary GJ 569BC and derived a total mass of $0.123 \pm 0.025 M_\odot$ for the two dwarfs. Lacking a dynamical measurement of the components’ mass ratio, they inferred a value of 0.89 from their relative near-infrared photometry of the pair.

likely” single-star parallax solution of 92.62 ± 1.52 mas (ESA 1997). Thus, the results of Uppgren & Harlow (1996) are probably not caused by unresolved duplicity.

3.6. Implications of New and Confirmed Companions

The companions described in this paper increase the number of known binary systems within 10 pc by 8% and the number of known systems within 10 pc having three or more components by 6% (T. Henry et al., in preparation). These new and confirmed systems can be grouped in several ways:

- Orbital periods $\lesssim 5$ yr (GJ 1001BC, GJ 54AB, and LHS 224AB)
- Component masses $\lesssim 0.15 M_{\odot}$ (GJ 1001BC, GJ 84B, LHS 224AB, and G 239–25B)
- Secondary/primary mass ratios $\lesssim 0.25$ (GJ 84AB and G 239–25AB)
- Secondary/primary mass ratios $\gtrsim 0.75$ (GJ 1001BC, GJ 54AB, and LHS 224AB)

Astrometrically monitoring the first group will quickly yield dynamic masses needed to constrain the MLR at well-spaced intervals between 0.50 and $0.05 M_{\odot}$. Monitoring the second group will extend the presently known MLR beyond its lower limit of $\sim 0.1 M_{\odot}$, where the effects of varying metallicity and age are pronounced (Baraffe et al. 1998). As members of the first two groups, GJ 1001BC and LHS 224AB merit immediate and comprehensive follow-up study. Indeed, GJ 1001BC offers one of the best opportunities to date for determining empirically the masses of binary brown dwarfs.⁶ GJ 84AB provides an opportunity for determining the mass of an M dwarf near the hydrogen-burning limit, but the system’s comparatively long period (~ 15 yr) requires a greater commitment of resources and patience than is needed for monitoring GJ 1001BC, GJ 54AB, and LHS 224AB. Unfortunately, an accurate measurement of the mass of the candidate brown dwarf G 239–25B probably will not be obtained within the lifetimes of current generations of astronomers.

Comparing the masses of GJ 1001BC with those of other short-period binary brown dwarfs having different spectral types (Table 7) will be the first steps toward empirically

⁶Bouy et al. (2004) recently determined a total dynamical mass of $0.146_{-0.006}^{+0.016} M_{\odot}$ for the L0+L1.5 binary 2MASS J07464256+2000321AB from its relative orbit. Using photometric and astrometric data and theoretical evolutionary tracks, they estimated masses of $0.085 \pm 0.010 M_{\odot}$ and $0.066 \pm 0.006 M_{\odot}$ for the L0 and L1.5 dwarfs, respectively.

mapping the cooling tracks of brown dwarfs with various masses. Moreover, by assuming that GJ 1001BC and other suspected substellar members of close-multiple systems [such as GJ 1245C (Henry et al. 1999), the M8.5–M9.5 dwarfs LHS 1070BC (Leinert et al. 2001) and GJ 569BC (Martín et al. 2000; Lane et al. 2001), the L dwarfs GJ 417BC (Bouy et al. 2003) and GJ 564BC (Potter et al. 2002), and the T dwarfs ϵ Indi BC (McCaughrean et al. 2004)] are coeval with their primary stellar companions, constraints can be placed on the often cited – but empirically untested – evolutionary models of brown dwarfs (Burrows et al. 1997; Chabrier et al. 2000).

The estimated mass ratios of the four binary M dwarfs are evenly distributed into low ($\lesssim 0.25$) and high ($\gtrsim 0.75$) bins. We can hardly draw statistical inferences from such a small sample, but it is interesting that the first identifications of binary M dwarfs from our NICMOS survey have a bimodal distribution of mass ratios. Such a distribution defies the noted tendency for binary M dwarfs to have components of approximately equal mass (Reid & Gizis 1997a,b). On the other hand, the nearly identical components of GJ 1001BC conform to the strong trend toward equal masses observed among binary L and T dwarfs (Reid et al. 2001; Burgasser et al. 2003; Bouy et al. 2003). We defer to a later paper a complete discussion of the systemic statistics (i.e., multiplicity fraction, secondary luminosity function, and distribution of mass ratios) of the RECONS “10 pc sample” once our NICMOS survey is complete and fully analyzed.

The authors thank Kuenley Chiu and Wei Zheng for obtaining the SPICam images of G239–25AB on our behalf. We also thank Mark Dickinson and Russet McMillan for their advice concerning the calibration of our NICMOS and SPICam data, respectively. Support for the NICMOS snapshot survey was provided by NASA through grants HST-GO-07420, HST-GO-07894, and HST-GO-09485 from the Space Telescope Science Institute (STScI). The FGS studies have been supported by NASA through grants HST-GO-08532, HST-GO-08729, HST-GO-09408, and HST-GO-9972 from the STScI. ACS was developed under NASA contract NAS5-32865, and ACS IDT research has been supported by NASA grant NAG5-7697 and by an equipment grant from Sun Microsystems, Inc. The STScI is operated by AURA, Inc., under NASA contract NAS5-26555.

Note added in proof – Resolved images of LHS 224AB and GJ 84AB have been published contemporaneously in *Astronomy & Astrophysics* by J.-L. Beuzit et al.

REFERENCES

- Bakos, G. A., Sahu, K. C., & Németh, P. 2002, *ApJS*, 141, 187
- Baraffe, I., Chabrier, G., Allard, F., & Hauschildt, P. H. 1998, *A&A*, 337, 403
- Basri, G., Mohanty, S., Allard, F., Hauschildt, P. H., Delfosse, X., Martín, E. L., Forveille, T., & Goldman, B. 2000, *ApJ*, 538, 363
- Blakeslee, J. P., Anderson, K. R., Meurer, G. R., Benitez, N., & Magee, D. 2003, *ASP Conf. Ser.* 295, *Astronomical Data Analysis Software and Systems XII*, eds. H. Payne, R. Jedrzejewski, and R. Hook (San Francisco: ASP), 257
- Bouy, H., Brandner, W., Martín, E. L., Delfosse, X., Allard, F., & Basri, G. 2003, *AJ*, 126, 1526
- Bouy, H., Duchêne, G., Köhler, R., Brandner, W., Bouvier, J., Martín, E. L., Ghez, A., Delfosse, X., Forveille, T., Allard, F., Baraffe, I., Basri, G., Close, L., & McCabe, C. E. 2004, *A&A*, 423, 341
- Burgasser, A. J., Kirkpatrick, J. D., Reid, I. N., Brown, M. E., Miskey, C. L., & Gizis, J. E. 2003, *ApJ*, 586, 512
- Burrows, A., Marley, M., Hubbard, W. B., Lunine, J. I., Guillot, T., Saumon, D., Freedman, R., Sudarsky, D., & Sharp, C. 1997, *ApJ*, 491, 856
- Campins, H., Rieke, G. H., & Lebofsky, M. J. 1985, *AJ*, 90, 896
- Chabrier, G., Baraffe, I., Allard, F., & Hauschildt, P. 2000, *ApJ*, 542, 464
- Close, L. M., Siegler, N., Freed, M., & Biller, B. 2003, *ApJ*, 587, 407
- Dahn, C. C., Harrington, R. S., Riepe, B. Y., Christy, J. W., Guetter, H. H., Kallarakal, V. V., Miranian, M., Walker, R. L., Vrba, F. J., Hewitt, A. V., Durham, W. S., & Ables, H. D. 1982, *AJ*, 87, 419
- Dahn, C. C., Harris, H. C., Vrba, F. J., Guetter, H. H., Canzian, B., Henden, A. A., Levine, S. E., Luginbuhl, C. B., Monet, A. K. B., Monet, D. G., Pier, J. R., Stone, R. C., Walker, R. L., Burgasser, A. J., Gizis, J. E., Kirkpatrick, J. D., Liebert, J., & Reid, I. N. 2002, *AJ*, 124, 1170
- Delfosse, X., Forveille, T., Beuzit, J.-L., Udry, S., Mayor, M., & Perrier, C. 1999, *A&A*, 344, 897

- Delfosse, X., Forveille, T., Ségransan, D., Beuzit, J.-L., Udry, S., Perrier, C., & Mayor, M. 2000, *A&A*, 364, 217
- Dickinson, M. E., et al. 2002, *HST* Data Handbook for NICMOS, Version 5.0, ed. B. Mobasher (Baltimore: STScI)
- ESA 1997, The *Hipparcos* and Tycho Catalogues, ESA SP-1200 (Noordwijk: ESA)
- Fischer, D. A., & Marcy, G. W. 1992, *ApJ*, 396, 178
- Ford, H. C., Clampin, M., Hartig, G. F., Illingworth, G. D., Sirianni, M., Martel, A. R., Meurer, G. R., McCann, W. J., Sullivan, P. C., Bartko, F., Benitez, N., Blakeslee, J., Bouwens, R., Broadhurst, T., Brown, R. A., Burrows, C. J., Campbell, D., Cheng, E. S., Feldman, P. D., Franx, M., Golimowski, D. A., Gronwall, C., Kimble, R. A., Krist, J. E., Lesser, M. P., Magee, D., Miley, G., Postman, M., Rafal, M. D., Rosati, P., Sparks, W. B., Tran, H. D., Tsvetanov, Z. I., Volmer, P., White, R. L., Woodruff, R. A. 2003, *Proc. SPIE*, 4854, 81
- Franz, O. G., Kreidl, T. J. N., Wasserman, L. W., Bradley, A. J., Benedict, G. F., Hemenway, P. D., Jefferys, W. H., McArthur, B., McCartney, J. E., Nelan, E., Shelus, P. J., Story, D., Whipple, A. L., Duncombe, R. L., Fredrick, L. W., & van Altena, W. F. 1991, *ApJ*, 377, L17
- Franz, O. G., Wasserman, L. H., Nelan, E., Lattanzi, M. G., Bucciarelli, B., & Taff, L. G. 1992, *AJ*, 103, 190
- Geballe, T. R., Knapp, G. R., Leggett, S. K., Fan, X., Golimowski, D. A., Anderson, S., Brinkmann, J., Csabai, I., Gunn, J. E., Hawley, S. L., Hennessy, G., Henry, T. J., Hill, G. J., Hindsley, R. B., Ivesić, Ž., Lupton, R. H., McDaniel, A., Munn, J. A., Narayanan, V. K., Peng, E., Pier, J. R., Rockosi, C. M., Schneider, D. P., Smith, J. A., Strauss, M. A., Tsvetanov, Z. I., Uomoto, A., York, D. G., & Zheng, W. 2002, *ApJ*, 564, 466
- Gizis, J. E., & Reid, I. N. 1996, *AJ*, 111, 365
- Gizis, J. E., Reid, I. N., & Hawley, S. L. 2002, *AJ*, 123, 3356
- Gliese, W., & Jahreiss, H. 1991, Preliminary Version of the Third Catalogue of Nearby Stars (Heidelberg: Astronomisches Rechen-Institut)
- Goldman, B., Delfosse, X., Forveille, T., Afonso, C., Alard, C., Albert, J. N., Andersen, J., Ansari, R., Aubourg, É., Bareyre, P., Bauer, F., Beaulieu, J. P., Borsenberger,

- J., Bouquet, A., Char, S., Charlot, X., Couchot, F., Coutures, C., Derue, F., Ferlet, R., Fouqué, P., Glicenstein, J. F., Gould, A., Graff, D., Gros, M., Haissinski, J., Hamilton, J. C., Hardin, D., de Kat, J., Kim, A., Lasserre, T., Lesquoy, É., Loup, C., Magneville, C., Mansoux, B., Marquette, J. B., Martín, E. L., Maurice, É., Milsztajn, A., Moniez, M., Palanque-Delabrouille, N., Perdereau, O., Prévot, L., Regnault, N., Rich, J., Spiro, M., Vidal-Madjar, A., Vigroux, L., & Zylberajch, S. 1999, *A&A*, 351, L5
- Golimowski, D. A., Henry, T. J., Krist, J. E., Schroeder, D. J., Marcy, G. W., Fischer, D. A., & Butler, R. P. 2000, *AJ*, 120, 2082
- Golimowski, D. A., Leggett, S. K., Marley, M. S., Fan, X., Geballe, T. R., Knapp, G. R., Vrba, F. J., Henden, A. A., Luginbuhl, C. B., Guetter, H. H., Munn, J. A., Canzian, B., Zheng, W., Tsvetanov, Z. I., Chiu, K., Glazebrook, K., Hoversten, E. A., Schneider, D. P., & Brinkmann, J. 2004, *AJ*, 127, 3516
- Golimowski, D. A., Nakajima, T., Kulkarni, S. R., & Oppenheimer, B. R. 1995, *ApJ*, 444, L101
- Goto, M., Kobayashi, N., Terada, H., Gaessler, W., Kanzawa, T., Takami, H., Takato, N., Hayano, Y., Kamata, Y., Iye, M., Saint-Jacques, D. J., Tokunaga, A. T., Potter, D., & Cushing, M. 2002, *ApJ*, 567, L59
- Hambly, N. C., Henry, T., Subasavage, J., Brown, M., & Jao, W.-C. 2004, *AJ*, 128, 437
- Harrington, R. S., Dahn, C. C., Kallarakal, V. V., Guetter, H. H., Riepe, B. Y., Walker, R. L., Pier, J. R., Vrba, F. J., Luginbuhl, C. B., Harris, H. C., & Ables, H. D. 1993, *AJ*, 105, 1571
- Hawley, S. L., Covey, K. R., Knapp, G. R., Golimowski, D. A., Fan, X., Anderson, S. F., Gunn, J. E., Harris, H. C., Ivesić, Ž., Long, G. M., Lupton, R. H., McGehee, P. M., Narayanan, V., Peng, E., Schlegel, D., Schneider, D. P., Spahn, E. Y., Strauss, M. A., Szkody, P., Tsvetanov, Z., Walkowicz, L. M., Brinkmann, J., Harvanek, M., Hennessy, G. S., Kleinman, S. J., Krzesinski, J., Long, D., Neilsen, E. H., Newman, P. R., Nitta, A., Snedden, S. A., & York, D. G. 2002, *AJ*, 123, 3409
- Henry, T. J., Franz, O. G., Wasserman, L. H., Benedict, G. F., Shelus, P. J., Ianna, P. A., Kirkpatrick, J. D., & McCarthy, D. W. 1999, *ApJ*, 512, 864
- Henry, T. J., Ianna, P. A., Kirkpatrick, J. D., & Jahreiss, H. 1997, *AJ*, 114, 388
- Henry, T. J., & McCarthy, D. W. 1990, *ApJ*, 350, 334

- Henry, T. J., & McCarthy, D. W. 1993, *AJ*, 106, 773
- Hinz, J. L., McCarthy, D. W., Simons, D. A., Henry, T. J., Kirkpatrick, J. D., & McGuire, P. C. 2002, *AJ*, 123, 2027
- Kirkpatrick, J. D., Liebert, J., Cruz, K. L., Gizis, J. E., & Reid, I. N. 2001, *PASP*, 113, 814
- Kirkpatrick, J. D., Reid, I. N., Liebert, J., Gizis, J. E., Burgasser, A. J., Monet, D. G., Dahn, C. C., Nelson, B., & Williams, R. J. 2000, *AJ*, 120, 447
- Knapp, G. R., Leggett, S. K., Fan, X., Marley, M. S., Geballe, T. R., Golimowski, D. A., Finkbeiner, D., Gunn, J. E., Hennawi, J., Ivesić, Ž., Lupton, R. H., Schlegel, D. J., Strauss, M. A., Tsvetanov, Z. I., Chiu, K., Hoversten, E. A., Glazebrook, K., Zheng, W., Hendrickson, M., Williams, C. C., Uomoto, A., Vrba, F. J., Henden, A. A., Luginbuhl, C. B., Guetter, H. H., Munn, J. A., Canzian, B., Schneider, D. P., & Brinkmann, J. 2004, *AJ*, 127, 3553
- Krist, J. E., Golimowski, D. A., Schroeder, D. J. & Henry, T. J. 1998, *PASP*, 110, 1046
- Krist, J. , & Hook, R. 2003, *The Tiny Tim User's Guide, Version 6.1* (Baltimore: STScI)
- Lane, B. F., Zapatero Osorio, M. R., Britton, M. C., Martín, E. L., & Kulkarni, S. R. 2001, *ApJ*, 560, 390
- Lang, K. R. 1980, *Astrophysical Formulae*, 2nd ed. (Berlin: Springer-Verlag)
- Leggett, S. K., Golimowski, D. A., Fan, X., Geballe, T. R., Knapp, G. R., Brinkmann, J., Csabai, I., Gunn, J. E., Hawley, S. L., Henry, T. J., Hindsley, R., Ivesić, Ž, Lupton, R. H., Pier, J. R., Schneider, D. P., Smith, J. A., Strauss, M. A., Uomoto, A., & York, D. G. 2002a, *ApJ*, 564, 452
- Leggett, S. K., Hauschildt, P. H., Allard, F., Geballe, T. R., & Baron, E. 2002b, *MNRAS*, 332, 78
- Leinert, C., Henry, T. J., Glindemann, A., & McCarthy, D. W. 1997, *A&A*, 325, 159
- Leinert, C., Jahreiss, H., Woitas, J., Zucker, S., Mazeh, T., Eckart, A., & Köhler, R. 2001, *A&A*, 367, 183
- Mack, J., et al. 2003, *ACS Data Handbook, Version 2.0* (Baltimore: STScI)
- Marcy, G. W., & Butler, R. P. 1998, *ARA&A*, 36, 57

- Marcy, G. W., Cochran, W. D., & Mayor, M. 2000, in *Protostars and Planets IV*, eds. V. Mannings, A. P. Boss, and S. S. Russell (Tucson: University of Arizona), 1285
- Martín, E. L., Delfosse, X., Basri, G., Goldman, B., Forveille, T., & Zapatero Osorio, M. R. 1999, *AJ*, 118, 2466
- Martín, E. L., Koresko, C. D., Kulkarni, S. R., Lane, B. F., & Wizinowich, P. L. 2000, *ApJ*, 529, L37
- Matthews, K., Nakajima, T., Kulkarni, S. R., & Oppenheimer, B. R. 1996, *AJ*, 112, 1678
- McCarthy, C., & Zuckerman, B. 2004, *AJ*, 127, 2871
- McCaughrean, M. J., Close, L. M., Scholz, R.-D., Lenzen, R., Biller, B., Brandner, W., Hartung, M., & Lodieu, N. 2004, *A&A*, 413, 1029
- McCaughrean, M. J., Scholz, R.-D., & Lodieu, N. 2002, *A&A*, 390, L27
- Meurer, G. R., Lindler, D., Blakeslee, J. P., Cox, C., Martel, A. R., Tran, H. D., Bouwens, R. J., Ford, H. C., Clampin, M., Hartig, G. F., Sirianni, M., & de Marchi, G. 2002, in *2002 HST Calibration Workshop*, eds. S. Arribas, A. Koekemoer, and B. Whitmore (Baltimore: STScI), 65
- Nelan, E., et al. 2003, *FGS Instrument Handbook, Version 12.0* (Baltimore: STScI)
- Nidever, D. L., Marcy, G. W., Butler, R. P., Fischer, D. A., & Vogt, S. S. 2002, *ApJS*, 141, 503
- Oppenheimer, B. R., Golimowski, D. A., Kulkarni, S. R., Matthews, K., Nakajima, T., & Creech-Eakman, M. 2001, *AJ*, 121, 2189
- Pavlovsky, C., et al. 2003, *ACS Instrument Handbook, Version 4.0* (Baltimore: STScI)
- Potter, D., Martín, E. L., Cushing, M. C., Baudoz, P., Brander, W., Guyon, O., & Neuhäuser, R. 2002, *ApJ*, 567, L133
- Reid, I. N., Cruz, K. L., Laurie, S. P., Liebert, J., Dahn, C. C., Harris, H. C., Guetter, H. H., Stone, R. C., Canzian, B., Luginbuhl, C. B., Levine, S. E., Monet, A. K. B., & Monet, D. G. 2003, *AJ*, 125, 354
- Reid, I. N., & Gizis, J. E. 1997a, *AJ*, 113, 2246
- Reid, I. N., & Gizis, J. E. 1997b, *AJ*, 114, 1992

- Reid, I. N., Gizis, J. E., Kirkpatrick, J. D., & Koerner, D. W. 2001, *AJ*, 121, 489
- Reid, I. N., Hawley, S. L., & Gizis, J. E. 1995, *AJ*, 110, 1838
- Riess, A. 2003, Instrument Science Report ACS 2003-009 (Baltimore: STScI)
- Rodgers, A. W., & Eggen, O. J. 1974, *PASP*, 86, 742
- Roye, E., et al. 2003, *NICMOS Instrument Handbook, Version 6.0* (Baltimore: STScI)
- Scholz, R.-D., Meusinger, H., & Jahreiss, H. 2001, *A&A*, 374, L12
- Simons, D. A., Henry, T. J., & Kirkpatrick, J. D. 1996, *AJ*, 112, 2238
- Sirianni, M., Clampin, M., Hartig, G. F., Rafal, M. D., Ford, H. C., Golimowski, D. A., Tremonti, C., Illingworth, G. D., Blouke, M. M., Lesser, M. P., Burmester, W., Kimble, R. A., Sullivan, P. C., Krebs, C. A., & Yagelowicz, J. 1998, *Proc. SPIE*, 3355, 608.
- Sirianni, M., et al. 2004, in preparation.
- Skrutskie, M. F., Forrest, W. J., & Shure, M. 1989, *AJ*, 98, 1409
- Teegarden, B. J., Pravdo, S. H., Hicks, M., Lawrence, K., Shaklan, S. B., Covey, K., Fraser, O., Hawley, S. L., McGlynn, T., & Reid, I. N. 2003, *ApJ*, 589, L51
- Tinney, C. G., Burgasser, A. J., & Kirkpatrick, J. D. 2003, *AJ*, 126, 975
- Upgren, A. R., & Harlow, J. J. B. 1996, *PASP*, 108, 64
- van Altena, W. F., Lee, J. T., & Hoffleit, E. D. 1995, *The General Catalogue of Trigonometric Stellar Parallaxes* (4th ed.; New Haven: Yale Univ. Obs.)
- Weis, E. W. 1988, *AJ*, 96, 1710
- Weis, E. W. 1996, *AJ*, 112, 2300
- Wilson, J. C., Kirkpatrick, J. D., Gizis, J. E., Skrutskie, M. F., Monet, D. G., & Houck, J. R. 2001, *AJ*, 122, 1989

Table 1. Dwarfs with newly discovered or confirmed companions

Name	RA	Dec	b ($^{\circ}$)	π (error) ^a (mas)	Proper motion		SpT	Photometry ^b			References ^c			
	(J2000)				μ ($''$ yr $^{-1}$)	PA ($^{\circ}$)		K_s	$V-K_s$	$J-K_s$	Coords.	π	μ	SpT
GJ 1001A	00:04:36.4	-40:44:03	-73	104.7 (11.4)	1.618	154.5	M3.5	7.74	5.10	0.86	1	2	3	4
GJ 1001B	00:04:34.9	-40:44:06	-73	104.7 (11.4)	1.618	154.5	L4.5	11.40	...	1.71	5	2	3	6
GJ 54	01:10:22.9	-67:26:42	-50	122.02 (6.04)	0.692	34.2	M3.0	5.13	4.67	0.88	7	2,7	7	8
GJ 84	02:05:04.8	-17:36:53	-71	106.37 (1.98)	1.329	97.5	M3.0	5.66	4.55	0.81	7	2,7	7	8
LHS 224	07:03:55.9	+52:42:06	+23	108.5 (2.1)	1.166	141.7	M5.0	7.78	5.51	0.76	1	2	3	9
G 239-25	14:42:21.6	+66:03:21	+47	101.34 (12.77)	0.316	259.2	M3.0	6.49	4.34	0.81	7	7	7	3

^aBased on weighted mean of referenced trigonometric parallaxes.

^b J and K_s from Two-Micron All Sky Survey (2MASS); V from Gliese & Jahreiss (1991) or Weis (1988, 1996).

^cReferences for coordinates, trigonometric parallax, proper motion, and spectral type: (1) Bakos, Sahu, & Németh 2002; (2) van Altena, Lee, & Hoffleit 1995; (3) Gliese & Jahreiss 1991; (4) Martín et al. 1999; (5) 2MASS; (6) Leggett et al. 2002b; (7) ESA 1997; (8) T. Beaulieu et al., in preparation; (9) Reid, Hawley, & Gizis 1995

Table 2. Log of observations

Item	GJ 1001A	GJ 1001B	GJ 54	GJ 84	LHS 224	G 239–25
Epoch 1						
Date (UT)	1998 Aug 03	2002 Oct 11	1998 Nov 09	2002 Oct 02	2003 Mar 13	1998 Nov 07
Telescope	<i>HST</i>	<i>HST</i>	<i>HST</i>	<i>HST</i>	<i>HST</i>	<i>HST</i>
Instrument	NIC2	NIC2	NIC2	NIC2	NIC2	NIC2
Program No.	7894	9485	7894	9485	9485	7894
Epoch 2						
Date (UT)	2003 Aug 20	2003 Aug 20	2000 Sep 24	...	2000 Jan 07 ^a	2003 May 06
Telescope	<i>HST</i>	<i>HST</i>	<i>HST</i>	...	<i>HST</i>	ARC 3.5 m
Instrument	ACS/HRC	ACS/HRC	FGS ^b	...	FGS ^b	SPICam
Program No.	9990	9990	8729	...	8532	...

^aObserved in independent FGS search for multiplicity among nearby M dwarfs and white dwarfs.

^bMonitoring of orbit continues as part of *HST* Programs 9408, 9972, and 10104.

Table 3. NIC2 exposure characteristics

Item	F110W	F180M	F207M	F222M
Mean λ (μm)	1.1035	1.7971	2.0786	2.2164
FWHM (μm)	0.5915	0.0684	0.1522	0.1432
MULTIACCUM sampling sequence ^a	STEP64	STEP64	STEP128	STEP128
<i>PHOTFNU</i> (Jy s DN ⁻¹ ; 62 K) ^b	1.86394e-6	1.07637e-05	5.38945e-06	5.11497e-06
<i>PHOTFNU</i> (Jy s DN ⁻¹ ; 77.1 K) ^c	1.2128 e-6	7.9701 e-06	4.2433 e-06	4.1897 e-06
F_ν (Vega) (Jy)	1898	932	735	653

^aSTEP n = 0.3, 0.6, 1, 2, 4, 8, ..., n (seconds).

^bValues before installation of NCS. (M. Dickinson 2004, private communication)

^cValues after installation of NCS. (M. Dickinson 2004, private communication)

Table 4. NICMOS photometry and astrometry of multiple systems

Name	Apparent magnitude (error) ^a				Method ^b	Separation (error)		PA (error) ^c (deg)
	F110W	F180M	F207M	F222M		Angular	Projected (AU)	
GJ 1001A	8.89 (0.04)	7.97 (0.04)	7.86 (0.04)	7.72 (0.04)	Aperture
GJ 1001B	14.50 (0.09)	12.86 (0.05)	12.47 (0.04)	12.04 (0.04)	PSF fit	0'087 (0'006)	0.83 (0.11)	48.1 (5.2) ^d
GJ 1001C	14.60 (0.09)	13.00 (0.05)	12.31 (0.04)	12.05 (0.04)	PSF fit			
GJ 54A	6.72 (0.12)	5.80 (0.05)	5.73 (0.05)	5.65 (0.05)	PSF fit	0'129 (0'006)	1.05 (0.07)	284.9 (3.8)
GJ 54B	7.28 (0.12)	6.59 (0.05)	6.51 (0.05)	6.37 (0.05)	PSF fit			
GJ 84A	6.38 (0.12)	5.75 (0.05)	5.55 (0.04)	5.57 (0.04)	PSF fit	0'443 (0'006)	4.17 (0.10)	103.4 (1.0)
GJ 84B	10.97 (0.09)	9.76 (0.05)	9.73 (0.04)	9.39 (0.04)	PSF fit			
LHS 224A	9.35 (0.12)	8.71 (0.09)	8.59 (0.09)	8.37 (0.09)	PSF fit	0'132 (0'012)	1.21 (0.11)	14.0 (7.2)
LHS 224B	9.36 (0.12)	8.88 (0.09)	8.75 (0.09)	8.51 (0.09)	PSF fit			
G 239-25A	7.66 (0.09)	6.74 (0.05)	6.68 (0.05)	6.59 (0.05)	PSF fit	3'041 (0'006)	30.01 (3.78)	114.0 (0.2)
G 239-25B	11.93 (0.04)	10.83 (0.04)	10.58 (0.04)	10.28 (0.04)	Aperture			

^aErrors include uncertainties in the following quantities, combined in quadrature (where applicable): photon noise, read noise, unsaturated PSF fits (3–8%), PSF fits affected by saturation or bad pixels (8%), absolute photometric calibration (< 3%), and zero point drift (< 2%).

^bMethod for determining integrated count rates (see §2.1).

^cPosition angle measured east of north.

^dPhotometric uncertainties make the identities of GJ 1001B and C ambiguous. Consequently, the PA suffers an ambiguity of 180°.

Table 5. FGS photometry and astrometry of binary M dwarfs^a

Name	$\Delta F583W$ (error)	Separation	PA (deg)	Epoch
GJ 54AB	1.040 (0.074)	0′11	93	2000.73
		0′13	283	2003.45
LHS 224AB	0.293 (0.006)	0′15	5	2000.02
		0′16	330	2003.83

^aPreliminary measurements of limited precision are given pending completion of the FGS monitoring programs. (See §2.2.1.)

Table 6. ACS photometry and astrometry of the GJ 1001 system

Name	Apparent magnitude ^a (error) ^b			Method ^c	Separation (error)		PA (error) ^d (deg)
	F625W	F775W	F850LP		Angular	Projected (AU)	
GJ 1001A	12.11 (0.02)	10.67 (0.02)	9.94 (0.02)	Aperture	18''.236 (0''.002) ^e	174.17 (18.96) ^e	258.8 (\ll 0.1) ^e
GJ 1001B	20.80 (0.04)	18.35 (0.07)	16.42 (0.11)	PSF fit	0''.086 (0''.002)	0.82 (0.09)	95.5 (0.5)
GJ 1001C	20.93 (0.04)	18.50 (0.07)	16.52 (0.11)	PSF fit			

^aAB magnitudes are given to permit comparison with SDSS r , i , and z photometry. To obtain Vega-based F625W, F775W, and F850LP magnitudes, subtract 0.167, 0.398, and 0.536, respectively, from the AB magnitudes listed in the table, and convolve an additional error of 0.02 mag to account for the uncertainty in the absolute flux calibration of Vega (Sirianni et al. 2004).

^bPhotometric errors include uncertainties in the following quantities, combined in quadrature (where applicable): photon noise, read noise, PSF fitting (3–10%), flat field (1%), instrument stability (0.5%), and charge-transfer inefficiency (1.5%).

^cMethod for determining integrated count rates (see §2.2.3).

^dPosition angle measured east of north.

^eSeparation and PA of GJ 1001BC's photocenter with respect to GJ 1001A.

Table 7. Known binary L and T dwarfs with periods $\lesssim 15$ yr

Name	SpT	Dist. (pc)	Separation (error)		Period ^a (yr)	References ^b		
			Ang.	Proj. (AU)		Image	SpT	π
GJ 1001BC	L4.5 + L4.5	9.6–15	0′087	0.8–1.3	3–5.5	1	2	3,4
2MASS J15344984–2952274AB	T5.5 + T5.5	13.6	0′065	0.9	3–5	5	5	6
2MASSW J0920122+351742AB	L6.5 + \sim L7.0	20.8 ^c	0′070	1.5	6–10	7	7	7
GJ 417BC ^d	L4.5 + \sim L5.5	21.7	0′070	1.5	7–11	8	9	10
2MASS J07464256+2000321AB	L0.0 + L1.5	12.2	0′12–0′22	1.5–2.7	8–13	7,11,12	12	13
GJ 564BC	L4.0 + L4.0	17.9	0′134	2.4	14–22	14	15	10
ϵ Indi BC	T1.0 + T6.0	3.6	0′732	2.6	15–25	16	16	10

^aPeriods of all binaries except 2MASS J0746+2000AB are estimated from equation (2) and assumed masses of 0.030–0.075 M_{\odot} (0.060–0.075 M_{\odot} for GJ 1001BC; see text). 2MASS J0746+2000AB’s period was computed by Bouy et al. (2004) from a Keplerian fit to 60% of its orbit.

^bReferences for resolved images, spectral types, and parallax: (1) this paper; (2) Leggett et al. 2002b; (3) van Altena, Lee, & Hoffleit 1995; (4) T. Henry et al., in preparation; (5) Burgasser et al. 2003; (6) Tinney, Burgasser, & Kirkpatrick 2003; (7) Reid et al. 2001; (8) Bouy et al. 2003; (9) Kirkpatrick et al. 2000; (10) ESA 1997; (11) Close et al. 2003; (12) Bouy et al. 2004; (13) Dahn et al. 2002; (14) Potter et al. 2002; (15) Goto et al. 2002; (16) McCaughrean et al. 2004.

^cEstimated from photometric parallax.

^dAlso known as 2MASS J1112257+354813AB.

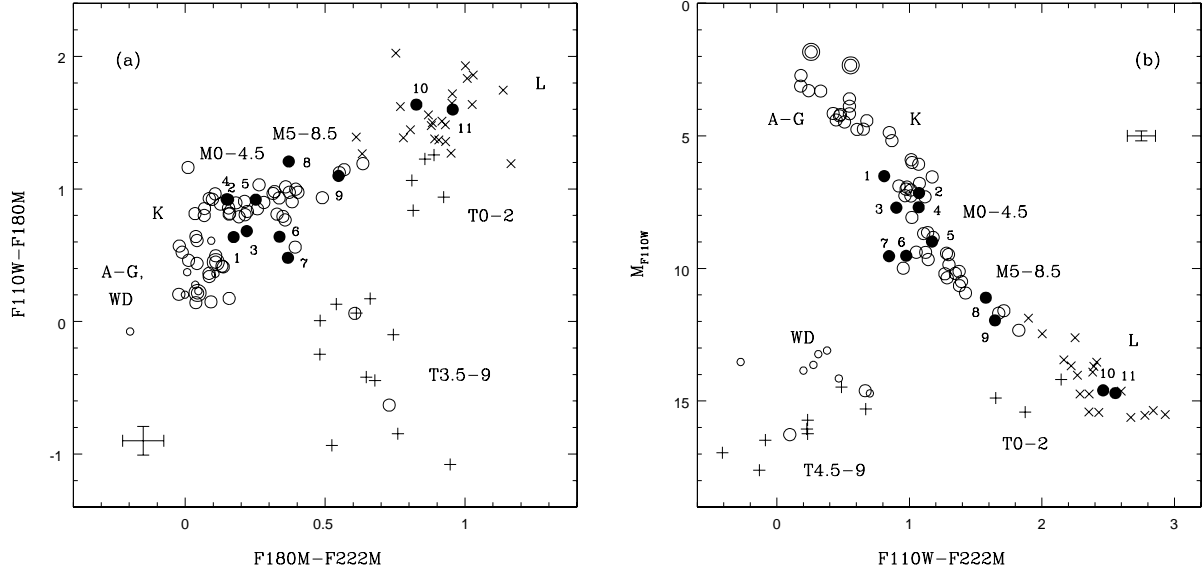


Fig. 1.— (a) NICMOS color-color diagram of $F110W-F180M$ versus $F180M-F222M$. (b) NICMOS color-magnitude diagram of M_{F110W} versus $F110W-F222M$. In each diagram, open circles represent stars and brown dwarfs within 10 pc imaged in our snapshot survey. (Large circles represent dwarfs with spectral types A through T, small circles represent white dwarfs, and concentric circles represent subgiants.) Filled and enumerated circles depict the following components of systems reported in this paper: (1) GJ 84A, (2) GJ 54A, (3) GJ 54B, (4) G 239-25A, (5) GJ 1001A, (6) LHS 224A, (7) LHS 224B, (8) GJ 84B, (9) G 239-25B, (10) GJ 1001B, and (11) GJ 1001C. Typical measurement errors for these nine dwarfs are shown in the lower-left corner of (a) and the upper-right corner of (b). The \times and $+$ symbols represent synthetic magnitudes and colors computed for L and T dwarfs, respectively. These values were obtained using flux-calibrated, near-infrared spectra (Geballe et al. 2002; Knapp et al. 2004), weighted-mean trigonometric parallaxes (Golimowski et al. 2004, and references therein), and the NICMOS Exposure Time Calculator produced by the Space Telescope Science Institute.

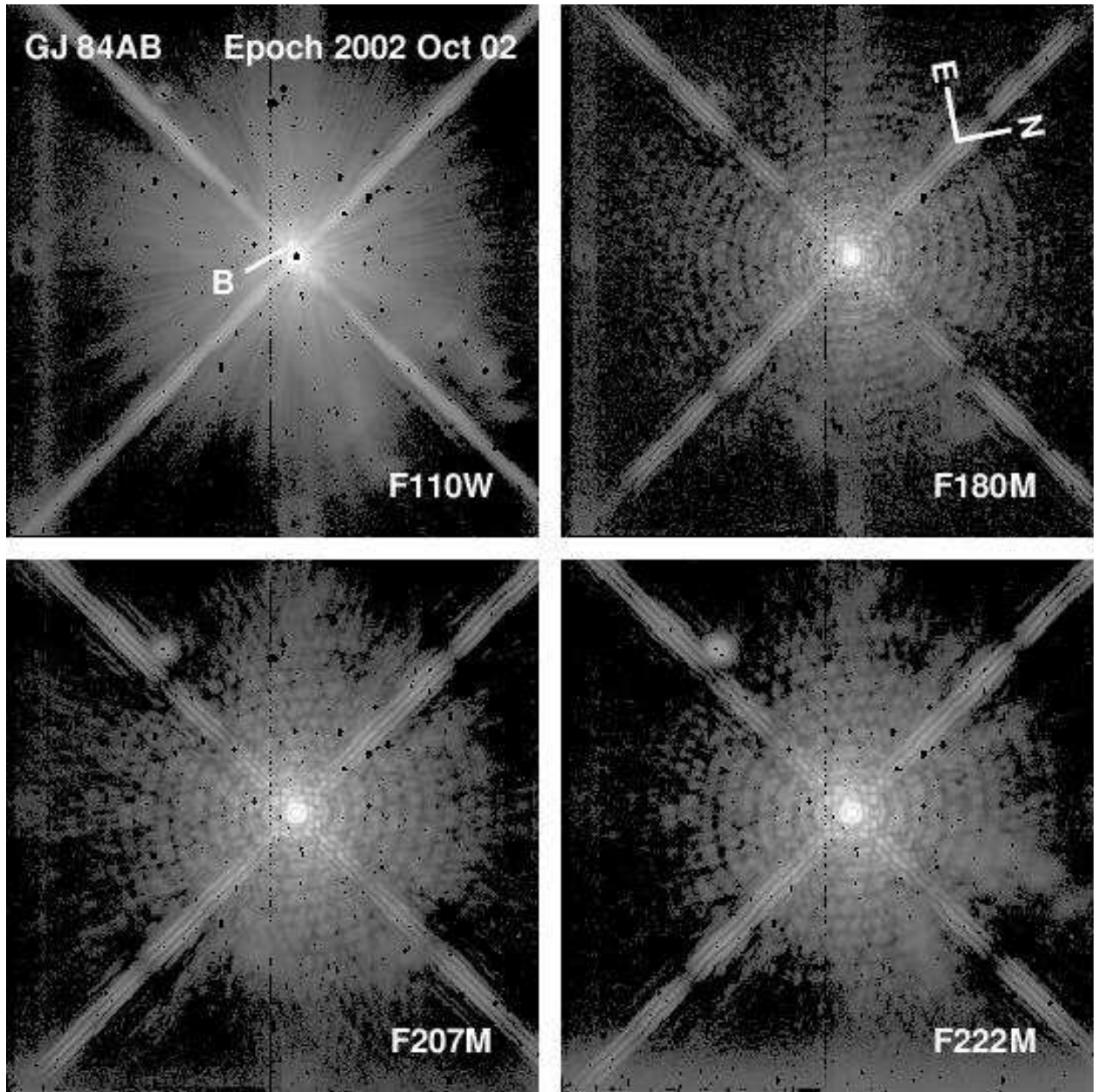


Fig. 2.— Reduced and calibrated NIC2 images of the binary M dwarf GJ 84AB. Each panel shows the full NIC2 FOV ($19''.5 \times 19''.5$) with logarithmic pixel scaling. The saturated core of the F110W image is marked with black pixels. The other black pixels denote intrinsically bad pixels and pixels affected by instrumental debris (“grot”) that has settled on the detector. The diffuse disks in the upper left quadrants of the images are flat-field artifacts caused by NIC2’s coronagraphic hole. The M7 V companion (*marked “B” in the upper left panel*), which lies $0''.44$ from the primary star along the southeast diffraction spike, is barely seen amid the highly structured PSF of the primary star.

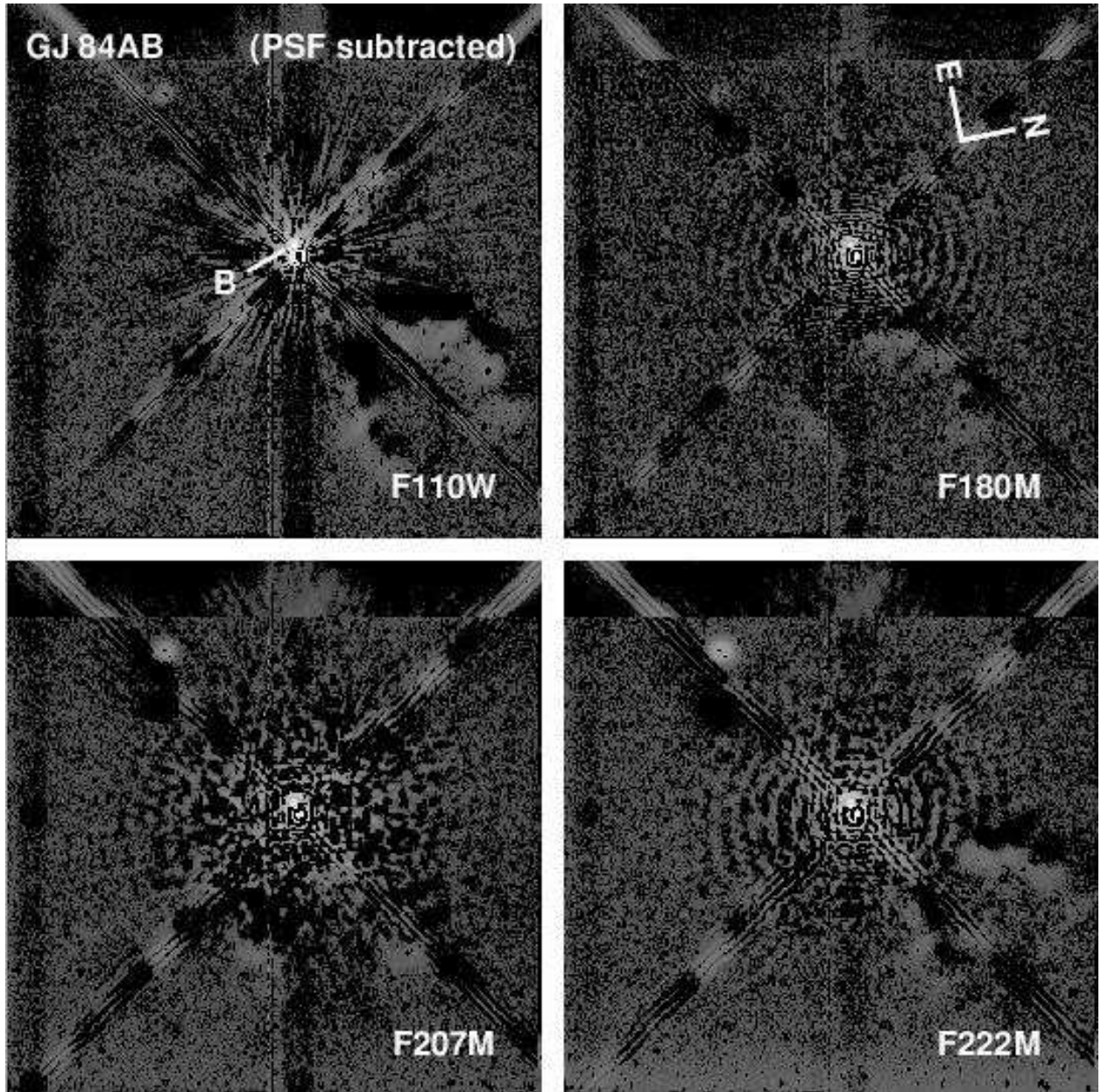


Fig. 3.— NIC2 images of GJ 84AB after optimal shifting, scaling, and subtraction of reference images of GJ 643 (M3.5 V) obtained on 2002 October 15. Each panel shows the full NIC2 FOV ($19''.5 \times 19''.5$) with logarithmic pixel scaling. The top 27 rows of each image are unaltered by the PSF subtraction because GJ 643’s image was located 27 rows higher than GJ 84’s image. The M7 V companion (*marked “B” in the upper left panel*) is evident in each panel immediately to the east of the central residuals of each subtracted PSF. No other sources appear in the FOV.

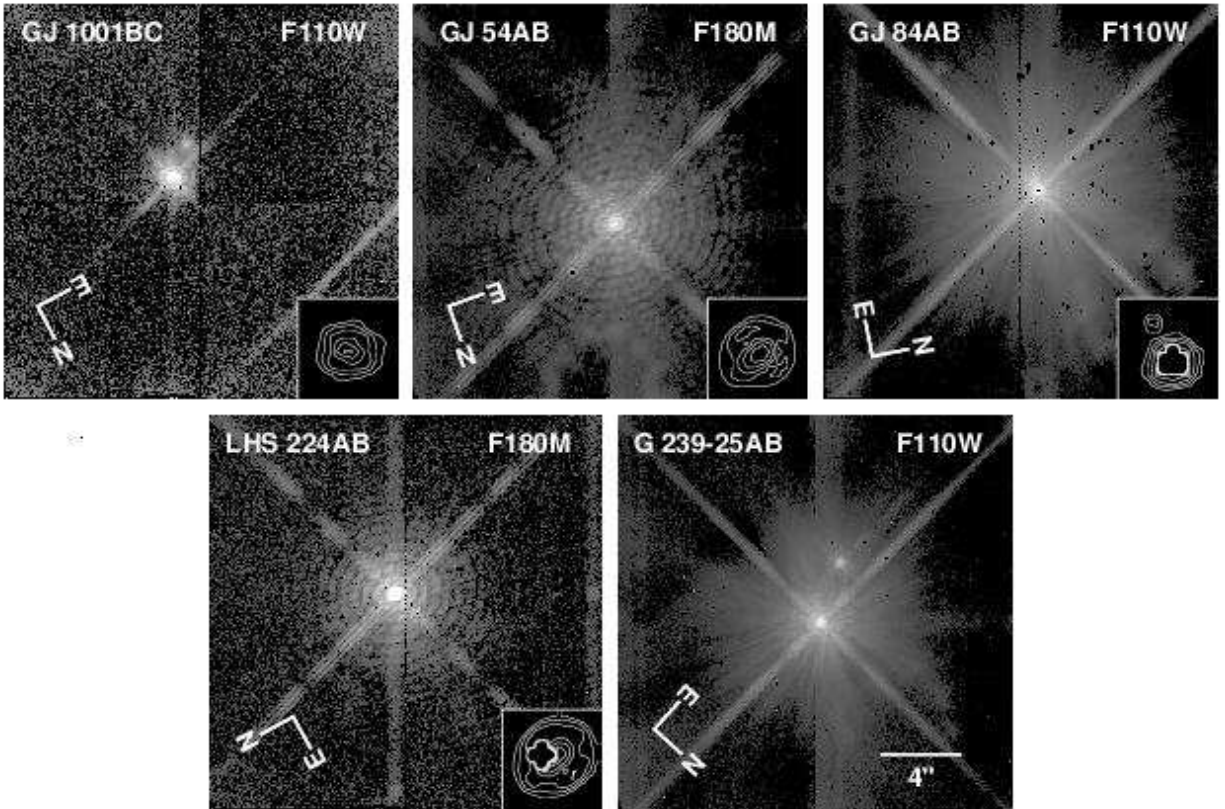


Fig. 4.— NIC2 images of the five dwarfs to which we have detected new or suspected companions. Each panel contains the filter image that most clearly shows the binary components. The full NIC2 FOV is displayed with logarithmic pixel scaling, except where masked by labels and insets. The insets show magnified contour plots of the 13×13 -pixel regions of each image centered on the close-binary dwarfs. Elongated contours indicate the orientations of the marginally resolved components. The images of GJ 84A and LHS 224AB are affected by overexposure and bad NIC2 pixels, respectively. The faint object located $1''.74$ to the southeast of GJ 1001BC is an extended source, presumably a background galaxy.

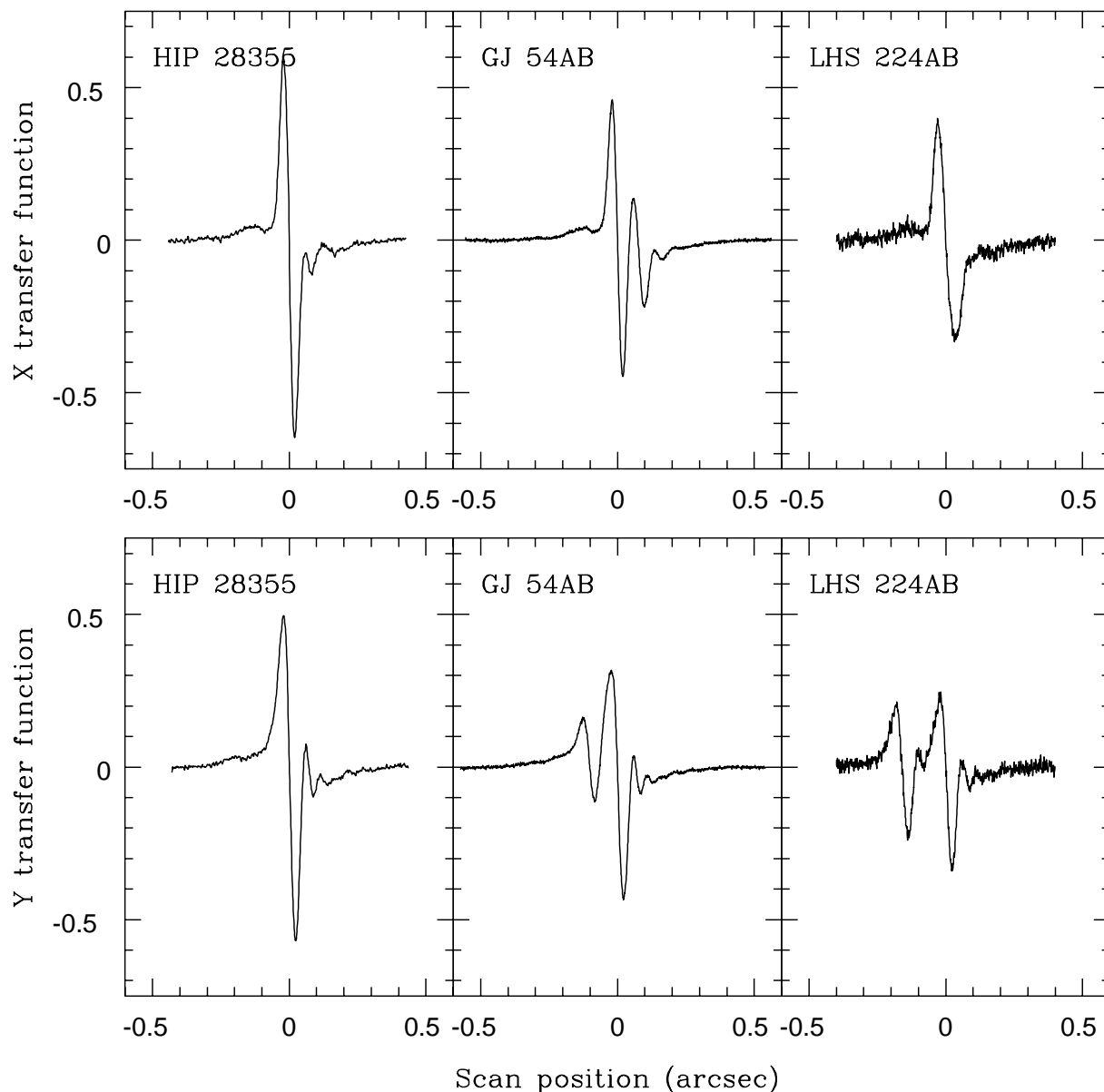


Fig. 5.— Broadband (F583W) FGS1r transfer functions of the single star HIP 28355 (*left panels*) and the binary stars GJ 54AB (*middle panels*) and LHS 224AB (*right panels*). The observations of GJ 54AB and LHS 224AB were obtained on 2003 June 13 and 2003 October 30, respectively. The transfer functions of single stars are generally antisymmetric about the zero scan positions with peak-to-peak amplitudes of ~ 1.2 ; asymmetric and/or diminished transfer functions reflect the presence of a secondary component. For instance, the right panels show that LHS 224A and B differ in brightness by 0.3 mag and are separated by $0''.03$ and $0''.16$ along the X and Y axes, respectively.

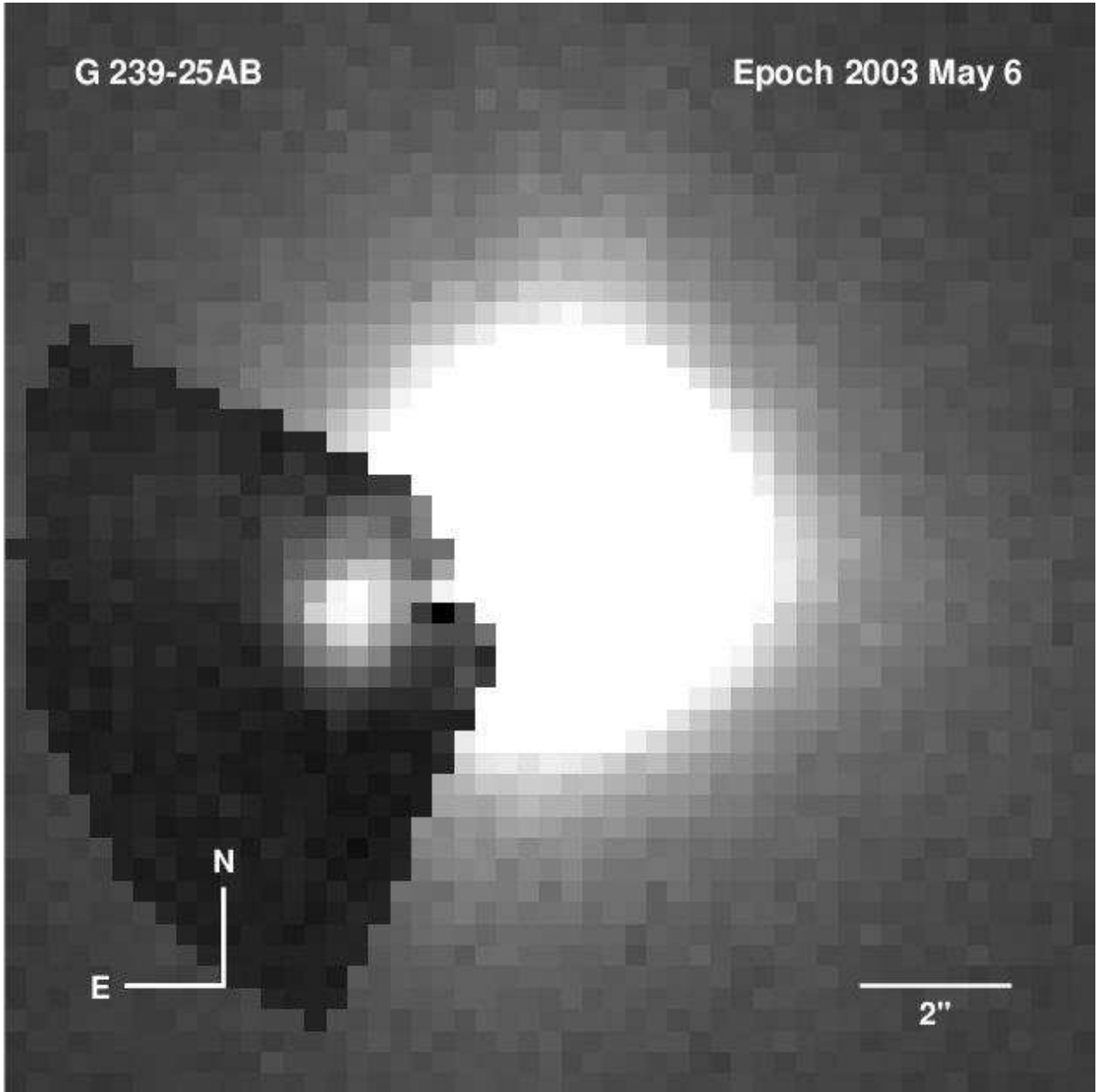


Fig. 6.— Image of G 239–25AB recorded through the SDSS z filter on 2003 May 06 using the ARC 3.5 m telescope and SPICam at Apache Point Observatory. This $14''.4 \times 14''.4$ region of the 1 s image is displayed with a linear scale and clipped at $1000 e^-$ to limit the dynamic range. The seeing-limited PSF of G 239–25A has been partly subtracted to reveal more clearly the faint companion located $2''.84$ to the east–southeast.

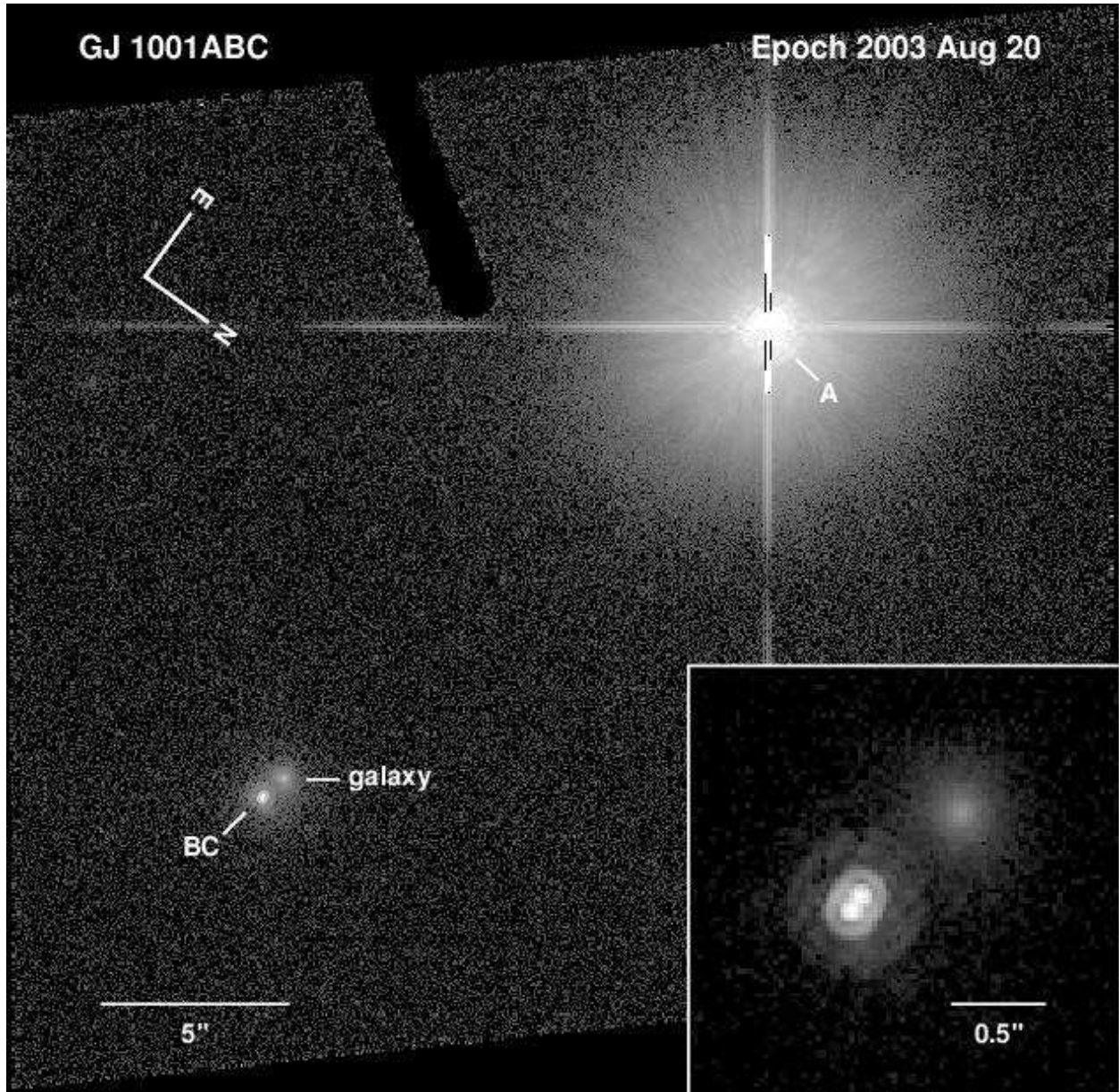


Fig. 7.— F775W (SDSS *i*) image of the GJ 1001 triple system obtained with the ACS HRC and processed by APSIS (see §2.2.3). The rhomboidal image is a geometrically corrected composite of two dithered 300 s HRC exposures. The binary L dwarf GJ 1001BC lies $\sim 18''.2$ from the M3.5 primary star GJ 1001A and $\sim 0''.75$ from the same anonymous galaxy seen in the NIC2 image (Figure 4). No other sources appear in this high-latitude ($b = -73^\circ$) field. The inset shows a magnified and rescaled region centered on GJ 1001BC and the galaxy. The position angle of GJ 1001BC has changed significantly since the NIC2 observation of 2002 October 11.